

Type	Values
High Voltage (HV)	69 kV, 115 kV, 138 kV, 161 kV, 230 kV
Extra High Voltage (EHV)	345 kV, 500 kV, 765 kV
Ultra High Voltage (UHV)	1100 kV, 1500 kV

Table 1 Typical transport levels

The transport stage is typically composed by point to points HV links between step-up and step-down or between step-down and step-down ESs. Those links bridge distances from tenths to several hundred kilometers. Taking into account investment issues, overhead lines are mainly implemented in a three 120 degrees shifted phases architecture, building them in a symmetrical way while trying to equally distribute both true and reactive power load [21].

HV networks have been designed to optimally transport energy and to minimize the losses. These losses, regarding energy transmission, are due mainly to two factors: ohmic resistance and leakage losses. One can try to reduce the former by increasing voltage and reducing current, but this approach will yield to an increase of the latter. A trade-off has to be found in order to keep those losses as low as possible.

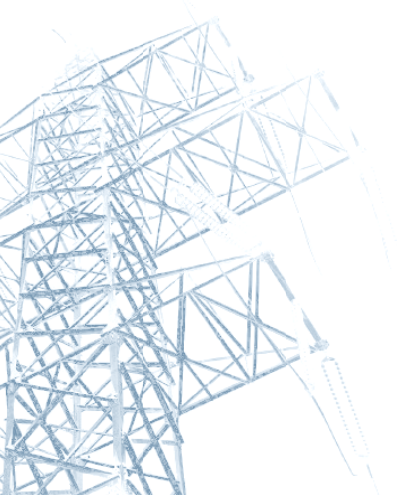
1. Ohmic resistance of the wire material.

The ohmic resistance depends on the conductor resistivity and on its magnetic permeability and the current frequency flowing in it. The influence of these parameters on the actual ohmic resistance is called skin effect that states that as frequency increases, the current distribution over the wire cross section is no longer constant, that is, there is a current displacement toward the wire surface [21].

2. Current leakage losses.

Basically, the leakage losses depend on the insulators' design and quality. These losses, in standard designs, are negligible in front the ohmic resistance. Related to this leakage of current, another kind of leakage losses can be found at HV levels: corona losses. These losses are caused by discharge activities of the wires, due to the presence of high electric fields. The strength of that discharges increases as the voltage level increases, as the wire diameter decreases and also increases with bad weather conditions. Bad weather, fog, rain, ice on the wires., increases the air conductivity thus causing stronger and more frequent discharges [23]. This effect, apart from causing energy losses, also introduces high frequency interference in the line, causing serious impairments to data communications systems. The corona noise effect can be reduced by using more than one wire or energy transport, instead of using only one [4].

If we focus on Radio Frequency (RF) transmission issues, some other considerations, apart from the ones stated before, should be taken into account in order to keep signal power attenuation as low as possible. This task is carried out by accurate impedance matching and signal driving through the HV lines. The former is done by means of coupling capacitors and matching or coupling units, while the latter is carried out by means of blocking coils or line traps, in order to route the data signal through the receiver (Figure 6).



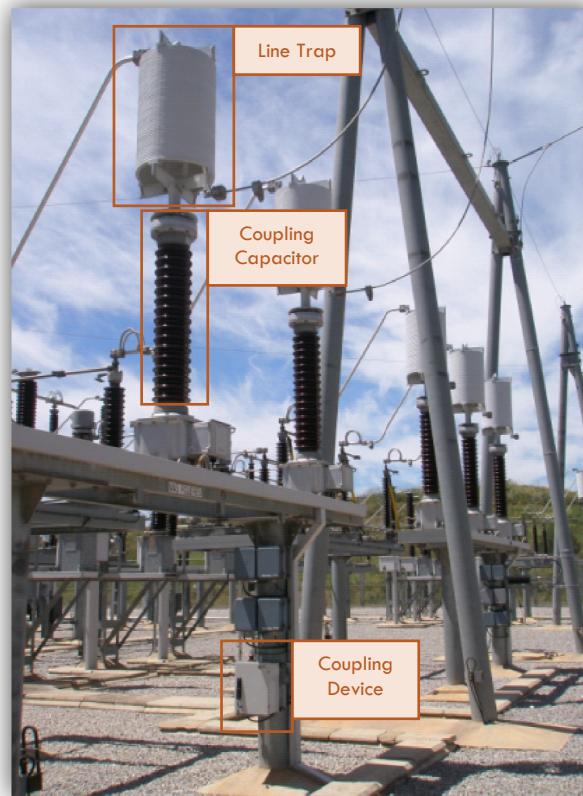


Figure 6 RF conditioning devices at Endesa “Egara” substation

At the beginning and at the end of the HV links, the line traps, usually based on 0.5 to 2 mH air-core coils, avoid the RF signal to enter the ES power switching and transforming area, thus, avoiding power losses. In order to couple the transmission equipment to the power line, 2 to 10 nF coupling capacitors are used. Between the communications equipment and the coupling capacitor, the coupling device, in charge of impedance matching and reflection avoidance, is located (Figure 7).

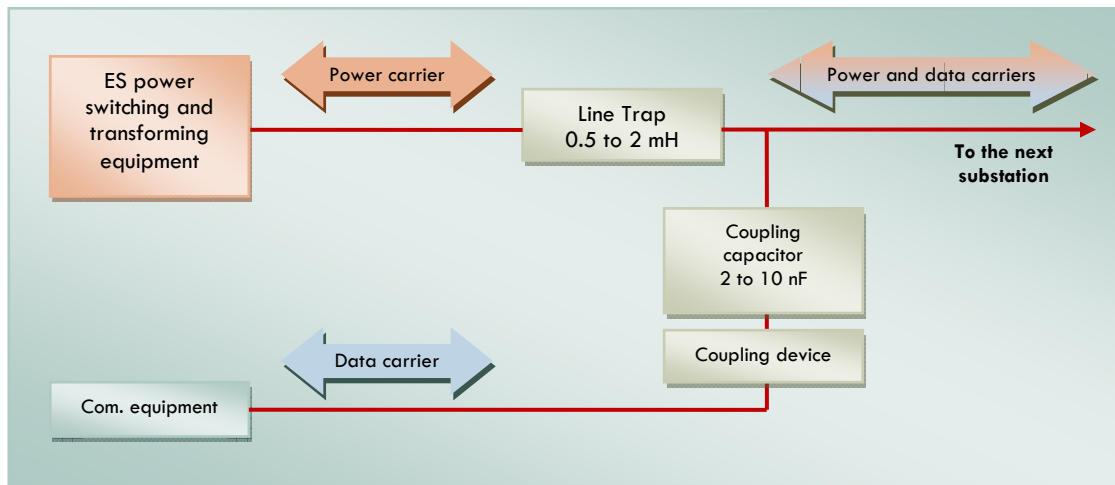


Figure 7 Line trap, coupling capacitor and coupling device in the HV network

When dealing with RF signals, the skin effect increases and corona noise is still present, but these are not the main attenuation factors. The main reason for power losses is the poor conductivity of the soil. Increasing with frequency, this attenuation is basically determined by the ratio between wire distance and the height of the same above the ground. In Table 2 the difference between the attenuation caused by the skin effect and the

one due to the soil are depicted for three different frequencies (for a ratio between the wire distance and the wire height of 3.5) [4].

Frequency	Skin Effect att. [dB/100 km]	Soil Effect att. [dB/100 km]
200 kHz	1.06	6.12
300 kHz	1.08	9.25
400 kHz	1.09	12.39

Table 2 Skin and soil effect attenuations

In conclusion, the following points have to be taken into account when designing communications equipment for the HV network (Figure 8) [24][25]:

1. Input impedance. Mainly affected by [4]:
 - a. Characteristic impedance of the transmission line.
 - b. Connected loads.
2. Noise scenario [4] [26]
 - a. Background colored noise: This type of noise is a broadband permanent interference with relatively high level and mainly caused by corona effect and other leakage or discharge events.
Background noise PSD is time and frequency variant. Due to climatic dependences, corona noise power fluctuations of 20 dB can be expected.
Stationary low-power periodical and synchronous with the mains impulse events can also be considered background noise. These kinds of impulses are caused by discharges on insulators and other ES devices.
 - b. Impulse events: This short duration noisy events have a broadband spectrum and usually a high level capable of represent a serious impairment to data communications and, even, for the equipment physical integrity as well. The main causes of this noise type are network switching transients (isolator switching or breaker operation) and lightning.
 - c. Narrowband noise: Narrowband interferences such a coupled broadcast emissions or other communications equipment are considered narrowband noise
3. Attenuation and frequency selectivity. Although it can happen with narrowband signals, especially when dealing with wideband signals, it is difficult for the coupling equipment to provide a good match in the whole transmission frequency range. If impedance matching is not good enough or there is some phase transposition (this can be seen as a sudden change of the line characteristic impedance) in the line, reflections can occur and multipath effects can appear making the channel frequency selective. Moreover, special attention has to be paid to the time spread and additional frequency selectivity caused by network elements, such as the coupling capacitors or the coupling devices.

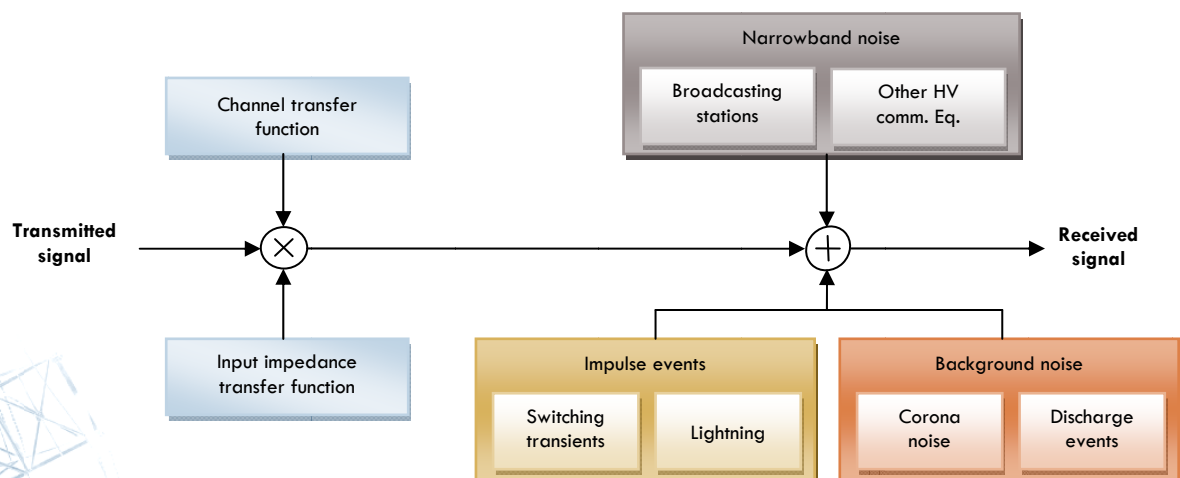


Figure 8 HV channel model

2.2. MEDIUM VOLTAGE NETWORKS

In conjunction with the LV network, the MV network comprises the distribution stage of the electric power grid. Located after the last step-down ES, and with typical levels of 6, 11 and 25 kV, the MV network feeds directly large commercial or industrial consumers and domestic and small commercial consumers through several TS.

The MV distribution system is characterized by the use of three phase configuration with the neutral often connected to the earth or ground. The MV networks can transport power in a single or double circuit basis. Single circuit consists on one line per phase, while double circuit transports power in two circuits per phase. The former structure can be found in low density and rural areas, while the latter, in high density areas or areas with special requirements. One line acts as a service line while the second acts as a backup. In urban areas, the MV network is fully underground, while in rural areas, both overhead and underground topologies can be found.

Regarding the urban underground MV distribution power grid, there are basically three topologies: star, ring and mesh. The star topology joins the ES with the TSs by means of one (Figure 9) or several radial lines that depart from the center of the star (the ES). These lines (or feeders) can be exclusive for one TS or cross several transformer substations. Moreover, these lines can be even branched (Figure 10).

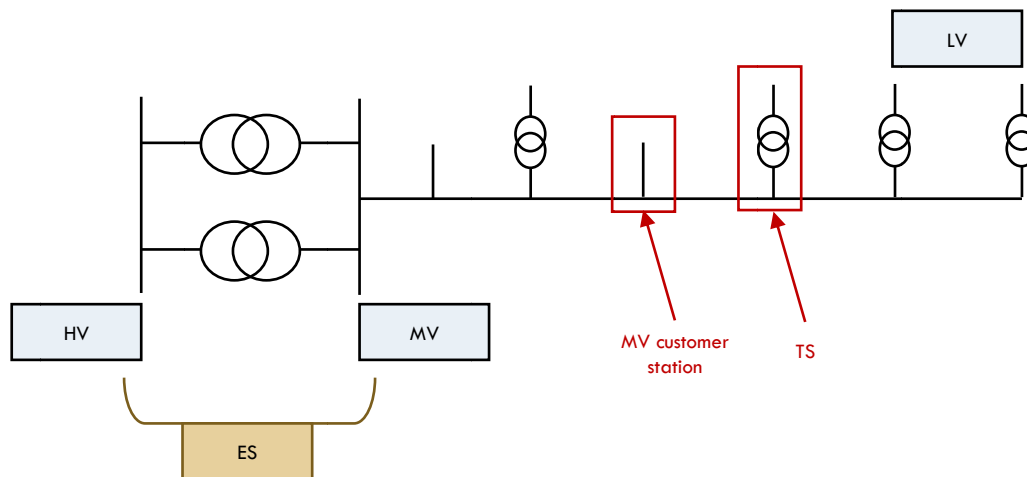


Figure 9 Star topology. A single MV line feeds MV customers and TS

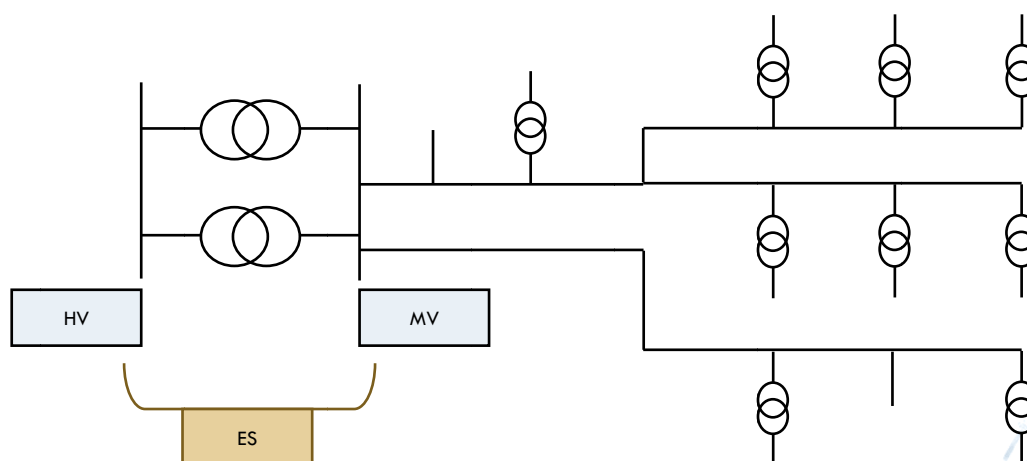


Figure 10 Star topology. Several MV lines with branching

In mesh topologies, the ES are joined by several MV lines, the power can be delivered by several routes: in case of a MV line failure, the power can be rerouted. Regarding mesh topology, complexity is the main drawback of this kind of architectures. Although in general, the MV networks are meshed EU operate them

as star topology, configuring the large complex meshed network into several star networks. Star topologies have several advantages over the meshed ones, like easier fault current protection and voltage control, easier prediction and control of power flows and lower cost; but if one segment of the MV line fails, it means interrupting the service beyond the point of failure.

In order to overcome the problem of star networks, an improved star topology named ring topology, consisting of two MV feeders departing from the ES, share a common point named the border of the ring. This border is an open circuit between the two radial MV lines. This border can be moved in order to limit the impact of a failure into the network, minimizing the length of the segment (and the number of TS) affected by the failure (Figure 11) [22].

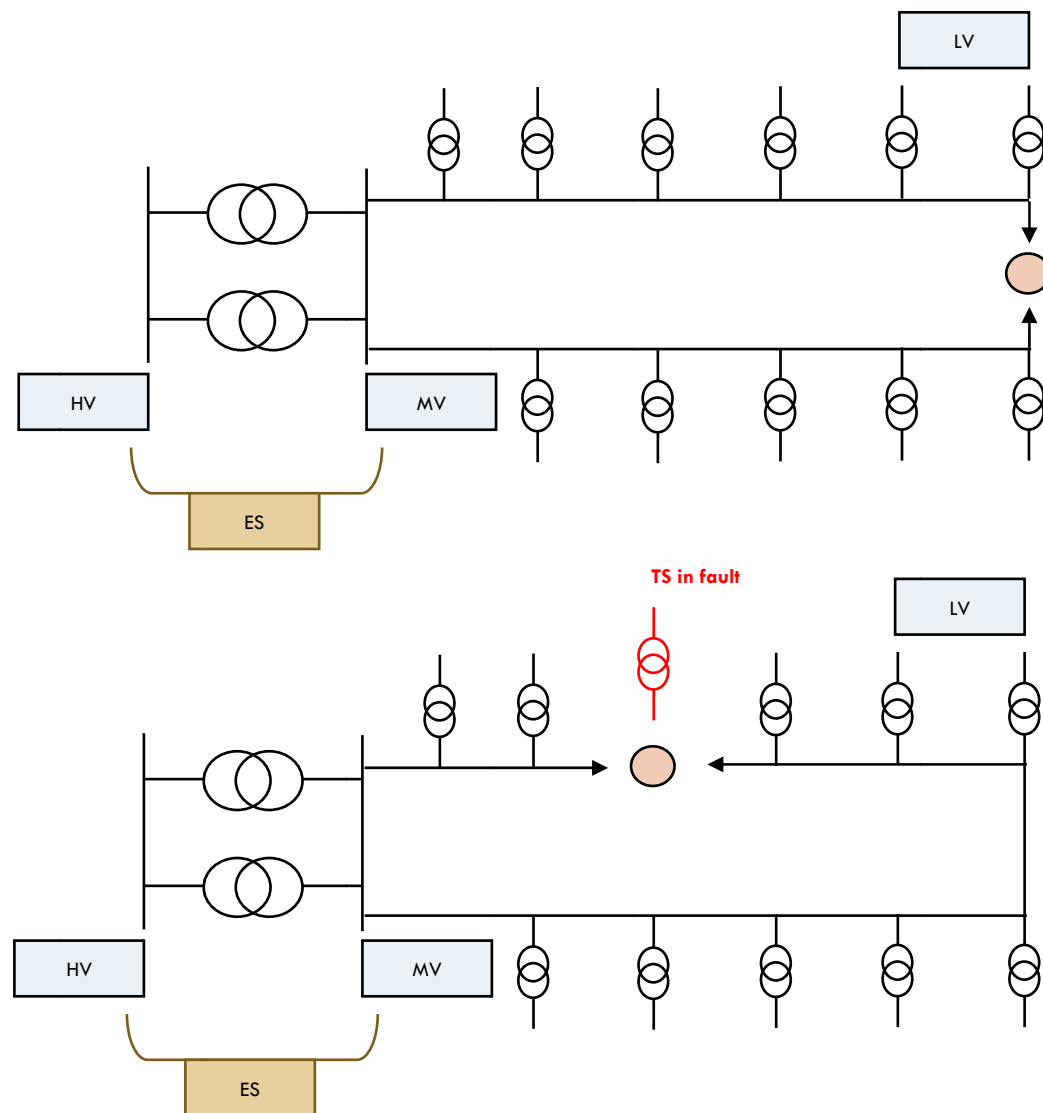


Figure 11 Ring topology in normal configuration and in fault configuration

The average number of TS per MV segment ranges from 4 to 30, with a typical number around 20. Each TS is separated from each other from 150 to 400 meters in urban areas, while in low density or rural areas this distance can increase up to 1000 meters. Usually, each TS outputs about 6 feeders to the LV customers which range from 200 to 500 meters, approximately.

Figure 12 shows the TS basic scheme. When the MV line enters the TS it has to pass through the input breaker and the output breaker to follow its way through the ring. In case of a failure in some TS, both input and output breakers will be opened in order to move the ring border to the faulty point.

In conjunction with the protection breaker, the input and output breaker are the typical topology configuration of the TS called ring main unit (RMU). If the MV to LV transformer is wanted to be in service, the RMU protection breaker has to be switched on.

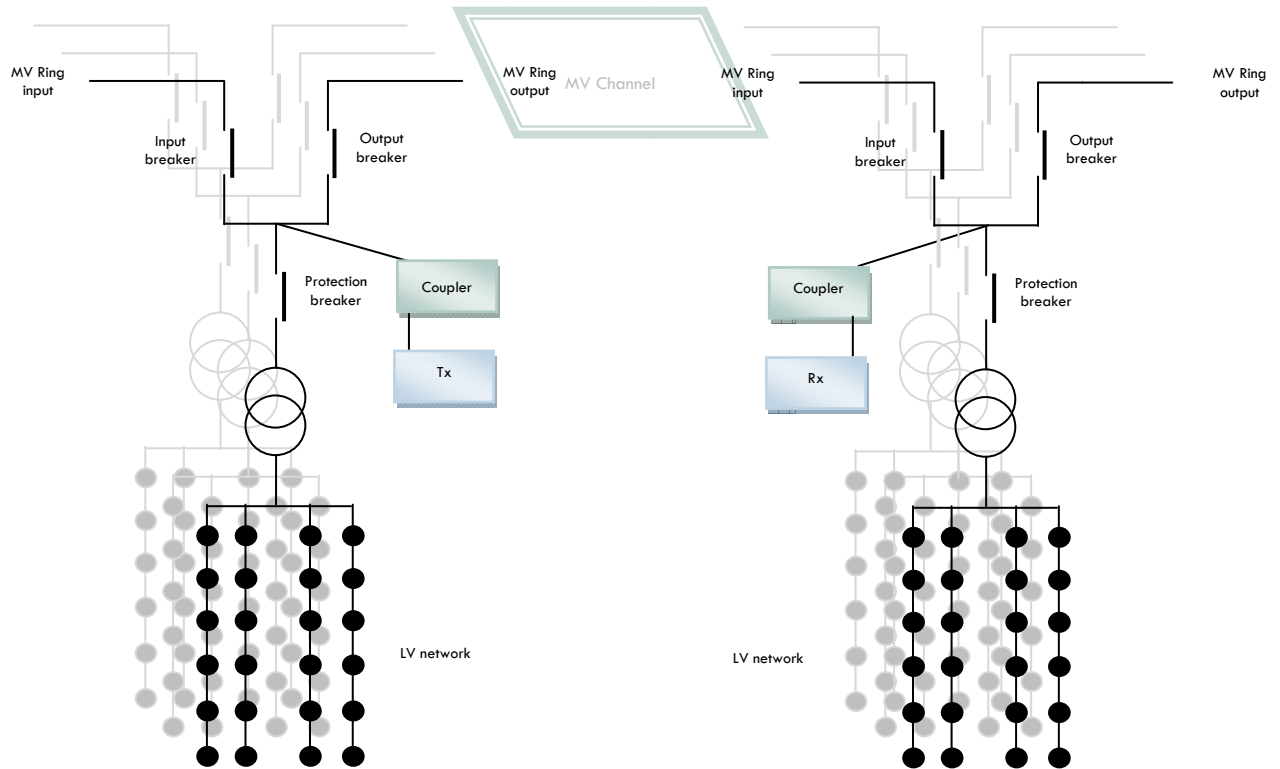


Figure 12 TS basic scheme

PLC signal is transmitted and received through the MV channel by means of capacitive (or inductive couplers). Typical coupling scheme is phase-to-ground. While in HV network the impedance matching and coupling elements are separate devices, in MV a single device couples and matches the impedance from the communications equipment to the MV channel input impedance, e.g., the PLCoupling / DIMAT CAMT capacitive coupler (Figure 13) has been designed in order to maximize the performance (in terms of transmission and reflection) taking into account an equipment output impedance of 50Ω and an expected line impedance of 20Ω [27].



Figure 13 MV Dimat CAMT capacitive coupling unit used in the measurements

The MV channel input impedance is not a constant value. Impedance value varies as a function of time, frequency and location. This variation, which is due to the changing loads connected to the MV network, is higher than the variations in HV lines but not so high as in LV ones. If channel access impedance is different from the one expected by the coupler, the injected power will be less than the optimum and undesirable reflections will occur. In HV channels, the coupling device offer some degree of freedom when matching equipment and channel impedances, usually, in MV channels, this possibility does not exist.

Near the mains frequency, the MV channel access impedance varies influenced by mains level, directly connected loads to the MV (large consumers), the connection and disconnection of other meshed MV feeders and the consumer loads connected to them. Otherwise, for frequencies over tens of kilohertz, HV/MV and MV/LV transformers are almost perfect barriers, so, high frequency signals are naturally confined within the MV network. Typically, high frequency signal attenuations from 60 to 80 dB can be expected from the transformer HV or LV side to the MV network [28]. The load fluctuation in that frequency range is due to the connection and disconnection of directly connected loads (large customers) and feeders, in the same way, interference coming from the HV and LV networks is heavily attenuated. On the other hand, if some kind of high frequency coupling between MV and LV or HV networks is needed, the MV properties will be determined by the LV network, in terms of interference and impedance [4][29][30].

Regarding MV cables, they can be classified into overhead and underground cables. The latter (Figure 14) can also be classified according several criteria, three of them are:

1. Number of conductors inside the cable: Unipolar, Tripolar.
2. Material of the conductor: Copper, Aluminium.
3. Type of insulation: XLPE (Cross-Linked Polyethylene), EPR (Ethylene Propylene Rubber), Oil paper.

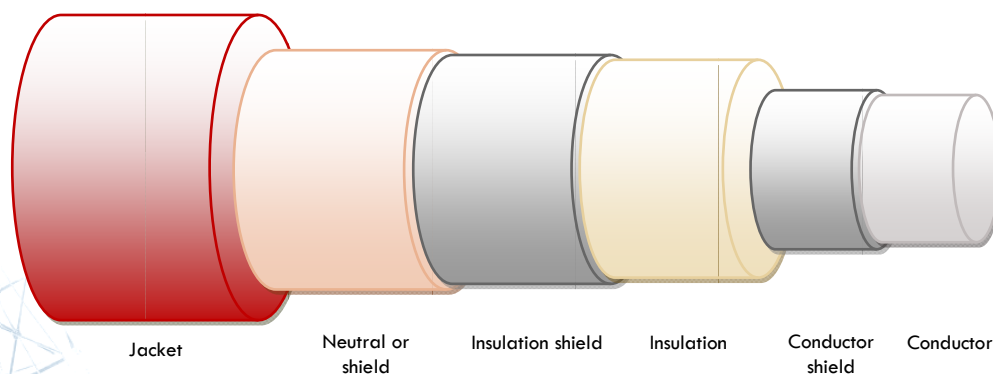


Figure 14 Unipolar underground cable structure

In Spain, EUs are now mainly deploying 25 kV unipolar aluminium XLPE cable in urban areas. XLPE cables have lower attenuation than EPR, which permits communication over longer distances. This type of cable has a characteristic impedance from 20 to 30 ohm approximately.

Regarding underground MV networks, the following channel effects have to be taken into account, and their model [24][25] can be seen in Figure 15:

1. Input impedance. Mainly affected by:
 - a. Characteristic impedance of the MV cable.
 - b. Connected feeder's loads.
2. Noise scenario.
 - a. Background colored noise: In MV networks, this noise is mainly caused by leakage or discharge events, power converters, transformer non idealities...
As well as in HV networks, stationary low-power periodical and synchronous with the mains impulse events can also be considered background noise. These kinds of impulses are caused by discharges on insulators and other ES or TS devices.
 - b. Impulse events: The main causes of this noise type are network switching transients (isolator switching or breaker operation) and lightning.
 - c. Narrowband noise: Narrowband interferences such a coupled broadcast emissions or other communications equipment are considered narrowband noise.
3. Attenuation and frequency selectivity. Caused by power dissipation or radiation and reflections in grid or coupling devices. These effects are included in the channel transfer function [4].

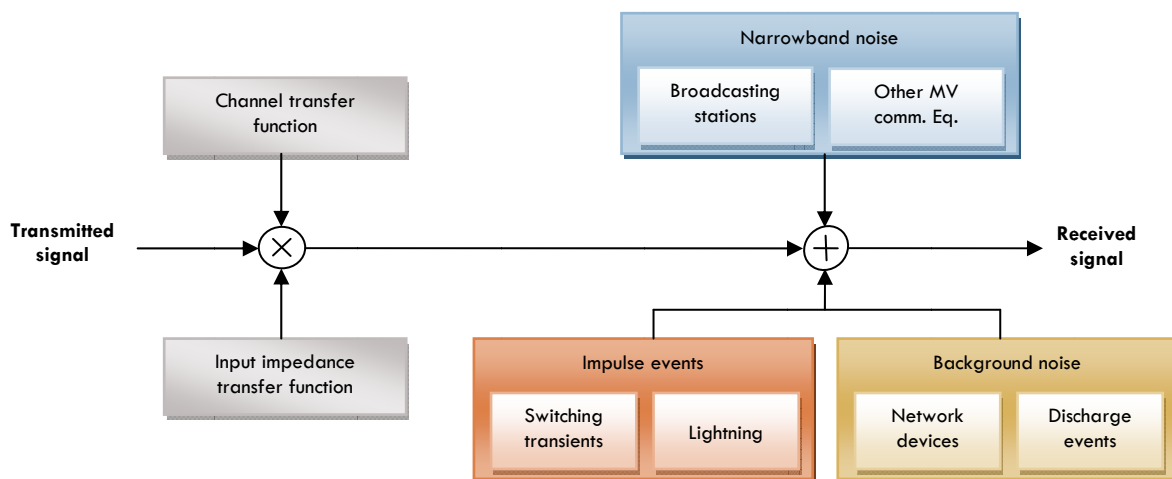


Figure 15 MV channel model

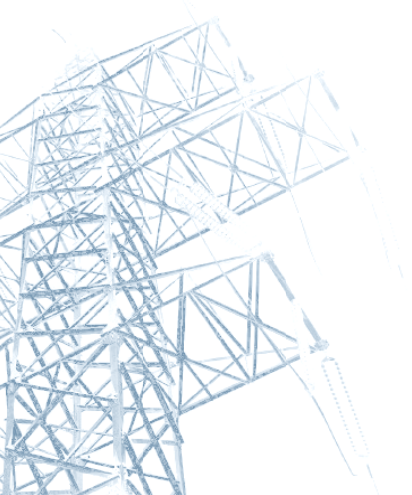
2.3. LOW VOLTAGE NETWORKS

The LV or secondary distribution network ranges from the TS to the final customer, typically, residential small commercial or industrial sites. With voltages below 1 kV (typical European configurations are 220 V phase to ground and 400 V phase to phase), the LV power grid has the most meshed and tree shaped power line topology of the whole power grid [22].

From the TS to the final customer, power flows through the following devices (Figure 16):

1. Once stepped-down, the mains goes into the switchboard. This device distributes the energy to the feeders by means of the busbars, a copper matrix that connects the input with the output of the switchboard. By the control unit, the switchgear selects the busbar interconnections. The breaker unit allows a safe manipulation of the switchboard by isolating it from the mains.
2. Once routed in the switchboard, the power goes toward the customers through 4 to 8 feeders

3. The LV lines can be classified in overhead lines (isolated and non-isolated) and buried cables. Overhead low voltage lines can be found in rural areas or small towns, as well as in areas with old buildings. In urban or relatively high density areas, the power is distributed by means of underground cables. The typical length for LV links (between the TS and the customer site) ranges from 50 to 300 meters.
4. Before reaching the customer, one line departing from the TS can go through one or several street cabinets. These cabinets are interconnection points between the meshed LV grid.
5. The fuse boxes are the points where the LV line EU property finishes and begin the line property of the customer. The function of these boxes is the protection of the EU distribution grid against any customer equipment malfunction or any other impairment that could affect the rest of the network. This protection is carried out by means of switches and fuses.
6. Usually located in the basement or in the ground floor, the meter room centralizes meters, protection and distribution devices. From the meter room, the (typical) single phase line goes towards the end user. In old buildings, instead of the meter room, there are copper bars called raisers. These raisers transport the power to the end-user premises (inside home), and this is the point where the meter is located, in a decentralized way.



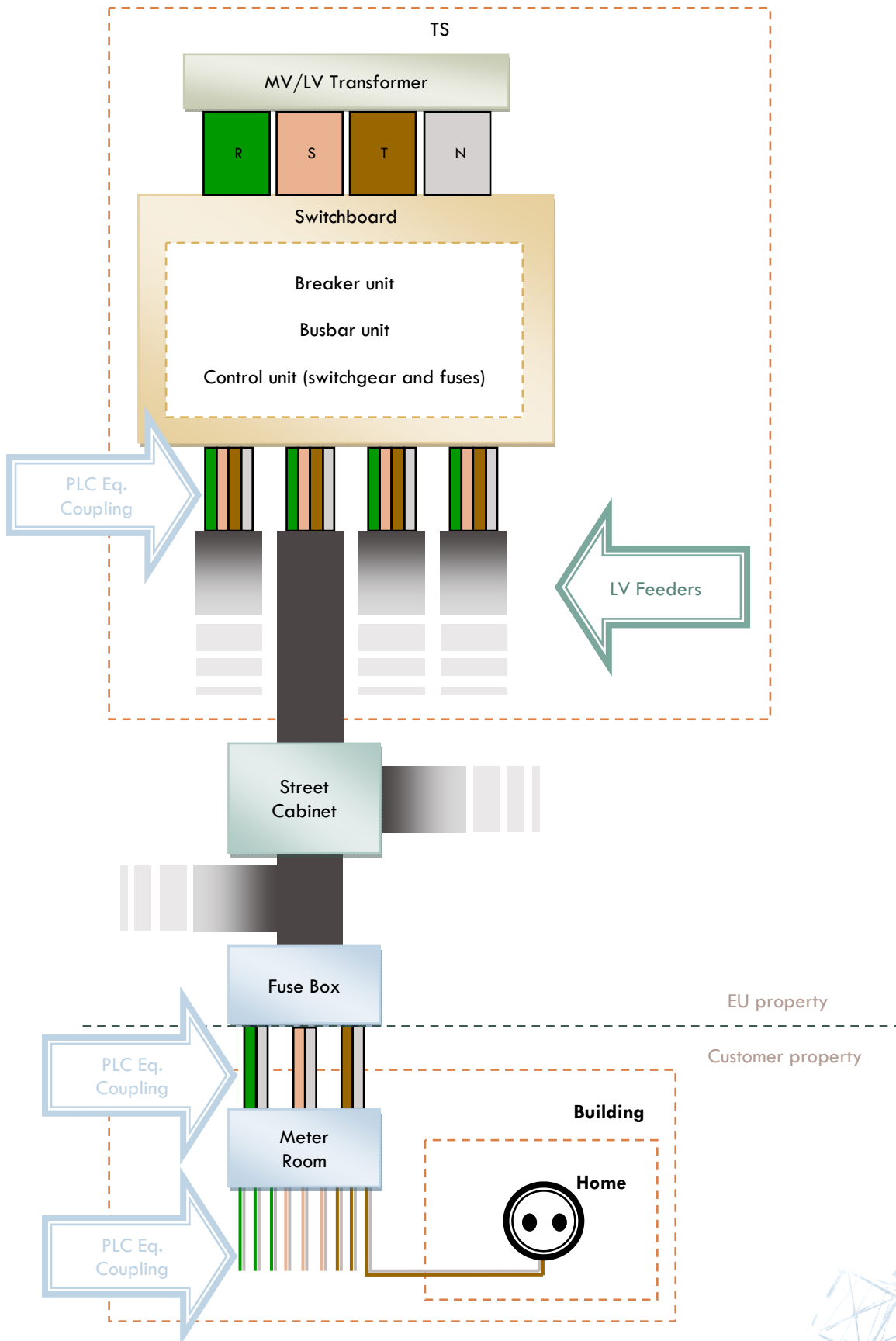
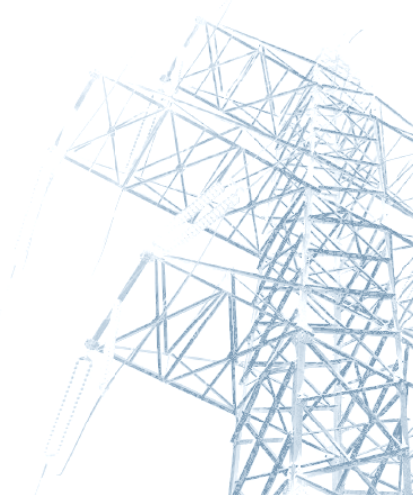


Figure 16 LV grid devices



The LV network shows a large branching and several reflection points, moreover, strong coupling between lines and/or phases can easily occur. Far from the HV network (that can be considered a reliable communications network) and even the MV network (whose radial lines are a quite good communications channel), the LV grid exhibit large frequency selectivity, high attenuation, high PSD background noise, specially at low frequencies, and high presence of impulsive events and a high time and frequency variability of the access impedance [31].

PLC in the LV network comprises three main types of applications:

1. Utility based command and control applications, e.g. AMR.
2. Last-mile (access) communications solution, also called broadband powerline communications (BPL).
3. In-home local area power line network.

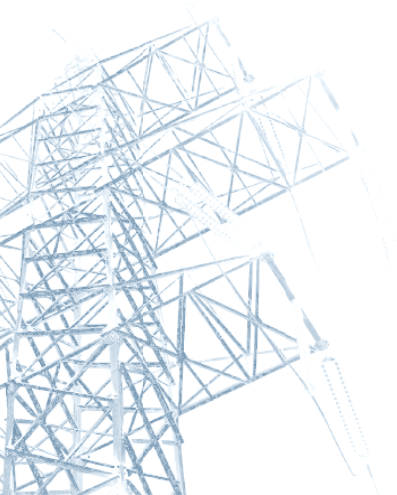
Although the former services can run over BPL, typical utility applications use the lower frequency range, i.e. below 1 MHz (utility reserved bands), with typical speeds around units of kbps. Regarding access and in-home solutions, with speeds around tens and hundreds of Mbps respectively, the broadband transfer function, noise scenario and access impedance vary both in time and frequency.

The tree shaped LV channel topology has several reflection points, like splices or terminations that, due to impedance mismatches, yields to a high frequency selective transfer function and an a-priori unknown access impedance. Since the termination impedance depends on the connected devices, it changes with the on/off switching of that devices and their own input impedance, changing the network transfer function and access impedance. These variations can be caused by human operation (long time variation) and by the device input impedance dependence on the mains voltage (short term variation) [55].

Far from being AWGN (Additive White Gaussian Noise), in the same way that HV and MV channels do, the LV network shows an even worst noise scenario. The LV noise can be classified in five types [24]:

1. Background noise
 - a. Colored background noise. This noise type is mainly caused by the summation of various low PSD time variant sources.
 - b. Narrowband noise. Due to the coupling of broadcast stations. Since it is slow variant it can be considered background noise.
 - c. Periodic impulsive noise asynchronous to the mains. Mainly caused by switched power supplies, this noise typically has a repetition rate from 50 to 200 kHz. Since it is slow variant it can also be considered background noise.
2. Impulsive noise
 - a. Periodic impulsive noise synchronous to the mains. With a repetition rate of 50 or 100 Hz, this type of noise is mainly caused by power supplies, and rectifiers. During these impulses, the PSD rises considerably over the background noise level.
 - b. Asynchronous impulsive noise. Caused by network switching transients, these impulses have a large PSD and a wide frequency presence.

Since the LV network presents the most complex noise scenario, the MV and HV channel models can be considered as simplified versions of the LV model (Figure 17):



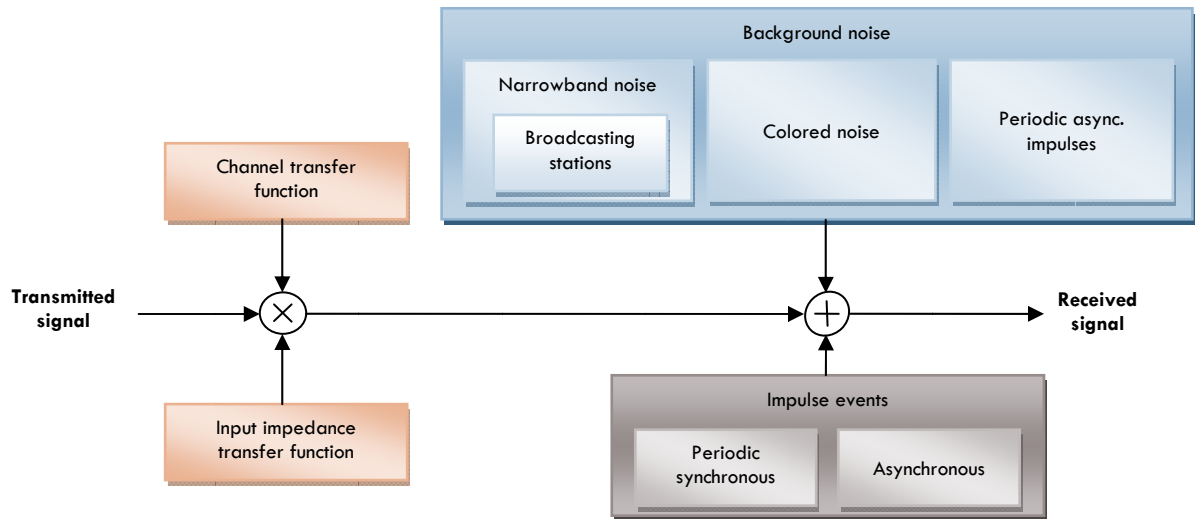
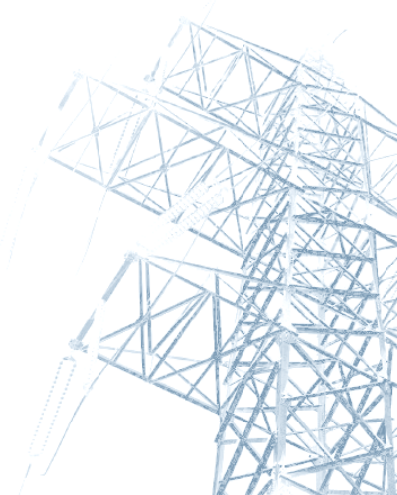


Figure 17 LV channel model



CHAPTER 3

3. AUTOMATIC METER READING AND LOW COMPLEXITY ROBUST MODEM DESIGN

In this chapter, the work regarding the LV power grid will be explained. The initial motivation for the research on LV came from a cooperation with Endesa Distribución Eléctrica S.L. The aim of this project was the study of the main theoretical proposals, as well as current implementations, of physical layer AMR systems. Then, based on that preliminary work and seeing the main drawbacks of the existing methods, the project yielded to a MCM based physical layer, allowing an increased data rate and a great level of frequency diversity, while keeping the system complexity relatively low.

3.1. INTRODUCTION

The introduction of an AMR system can offer several advantages related to the capacity of sending and receiving data between the customer and the EU. Apart from its natural application of electrical power consumption metering [40], other kinds of information can be also interesting, e.g.: time of use, consumption peaks, load balancing, remote control, load connection and disconnection, dynamic billing, fraud detection, etc [39]. Given a LV tree, LV-PLC connects the residential meters to their related concentrator or HE and the latter sends that information to the processing center [33][34].

From an EU point of view, PLC is the most suitable technology for AMR applications, because it is using an already deployed infrastructure, thus reducing deploying and maintenance costs since the power grid is usually owned by of the same entity that exploits the AMR technology.

In Europe, the standard CENELEC 50065 rules the use of the frequency range from 3 to 148.5 kHz, as well as the maximum levels that can be injected into the network. This frequency range is divided in four bands: the A band, from 9 to 95 kHz, restricted for the EUs and their licensers; and the B, C and D bands for private use. The maximum allowed level for those three bands is 122 dB μ V, while regarding the A band, the maximum level is 134 dB μ V in the whole frequency range or a decreasing level from 134 dB μ V to 120 dB μ V, for wideband or narrowband signals respectively (Figure 18).

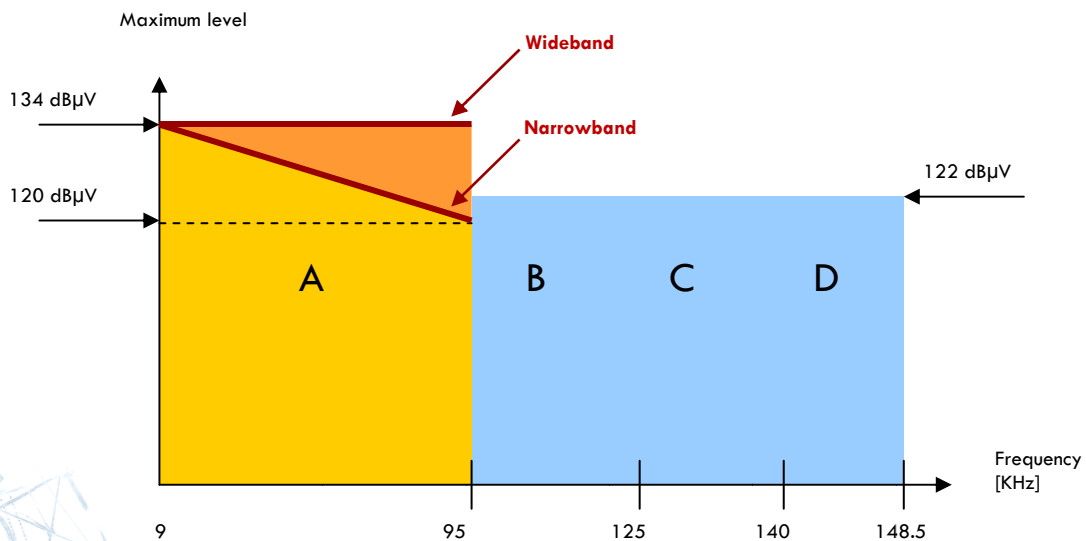


Figure 18 CENELEC band maximum levels

These levels are defined as the peak levels at the 100 Hz filter output, measured as stated in the standard. A given physical layer can be considered as a wideband modulation if its spectrum is 5 kHz wide or more.

There is no medium access mechanism defined by the standard, but for the C band, where Carrier Sense Multiple Access is used [13].

Typical characteristics of low frequency (up to 500 kHz) LV-PLC channels are a time and frequency dependent access impedance, an increasing attenuation with increasing frequency, a highly colored background noise, specially at low frequencies, and a complex impulsive noise scenario. For details about the characteristics of this channel the reader is referred to [49] and [86].

3.2. SUITABLE MODULATIONS FOR CENELEC A BAND

Narrowband modulations are a good choice if we face a friendly channel, i.e. flat or frequency non selective, AWGN only, without interference and with good SNR available at the receiver. On the other hand, wideband modulations are characterized by using a transmission bandwidth larger than the channel coherence bandwidth. Typical wideband modulations are MCM, spread spectrum (SS) and their combinations, known as MC-SS (multicarrier – spread spectrum) [16]. Regarding the CENELEC A band frequency range, one can say that it does not make sense to use wideband modulations, since the channel transfer function is almost flat. However, if we focus on the noise plus interference scenario, a new kind of frequency selectivity arises. This selectivity is caused by colored noise and impulse interferences in the frequency domain (in this context, wideband modulations make sense in the A band) and by impulsive noise in the time domain. Moreover, as stated before, wideband modulations can take advantage over narrowband schemes since the maximum allowed level is 134 dB μ V in the whole band [38][41].

3.2.1. NARROWBAND MODULATIONS

Based on a carrier property modification, i.e. amplitude, frequency or phase, one can define the following digital modulations: ASK, FSK and phase shift keying (PSK) respectively, as well as QAM if both amplitude and phase are modified simultaneously [42].

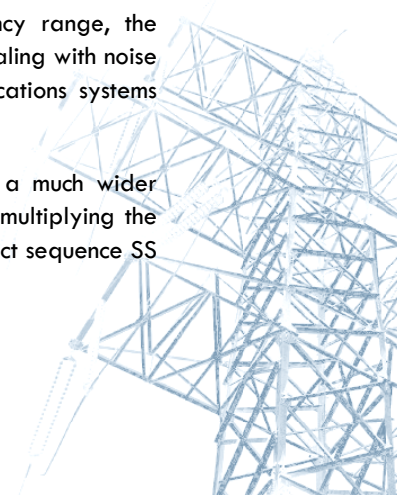
Historically, due to its simplicity and low cost, the ASK has been the choice for data transmission in LV-PLC channels. Robustness is not an outstanding characteristic of amplitude modulations, since variations in the received amplitude or the presence of interferers can severely affect the demodulator performance.

Better results can be obtained using phase modulations. The PSK, and specifically, the binary-PSK (BPSK), presents a great robustness in front of amplitude variations, but in the early times of narrowband low frequency systems, the FSK was the preferred access scheme since it has an easy implementation in both analog and digital systems. Usually, in order to decrease the undesirable out of band emissions, the FSK is implemented with continuous phase. Although a frequency corruption is much less probable than an amplitude corruption, FSK demodulation errors are mostly caused by narrowband interferences masking one or several FSK subcarriers [4][36].

3.2.2. WIDEBAND MODULATIONS

The robustness in front multipath effects and narrowband interferences has made the wideband modulations the choice for several communication systems [16]. Focusing on the CENELEC A frequency range, the multipath effects can be neglected, but SS and MCM can still be a good alternative when dealing with noise frequency selectivity, narrowband interferences or interferences caused by other communications systems [41].

The principle of SS techniques is to spread a signal in the frequency domain occupying a much wider bandwidth than minimum required for the transmission. Spreading can be accomplished by multiplying the original signal with a wideband signal (code) which is independent from the data, named direct sequence SS



(DS-SS) or by continuously changing the carrier frequency following a specific hopping pattern, named frequency hopping SS (FH-SS).

The first SS proposals were based on FH-SS [35][37]. This wideband modulation scheme is based on a typical narrowband modulation (in PLC, usually FSK) whose carrier frequency varies along time. This variation is defined in a pseudorandom noise (PN) sequence. Two types of FH-SS exist. If the hopping frequency is faster than the narrowband modulation symbol frequency, it is called fast FH-SS. Otherwise, if the hopping frequency is equal or lower than the symbol rate, it is called slow FH-SS. By hopping the narrowband modulation among a larger frequency range, the robustness against narrowband interferences is improved [42].

The other type of SS modulation is called DS-SS, where a PN sequence of L chips of duration T_c is time multiplied by the narrowband data symbols of duration T_d , yielding to a frequency spread version of the original data symbols (Figure 19).

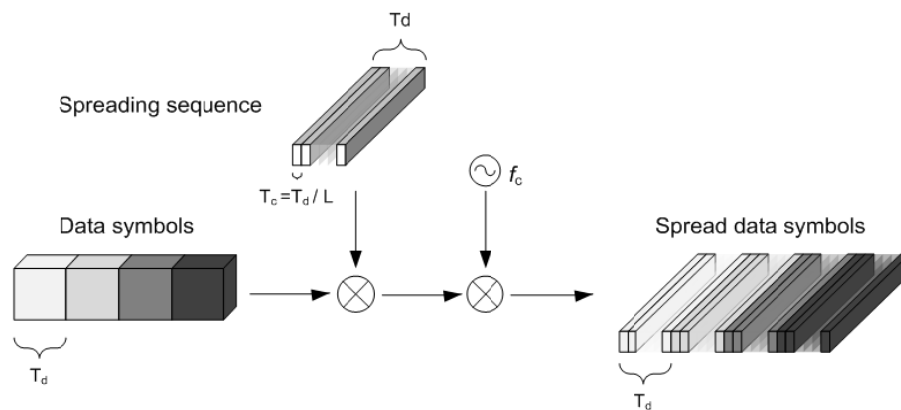


Figure 19 DS-SS modulation scheme

The ratio between the spread data symbol bandwidth and the data symbol bandwidth is called processing gain. This processing gain is a measure of how robust are the data symbols in front of narrowband interferences when traveling through the channel [42].

If focusing in A band applications such as AMR, the highest frequency range is often used to transmit data, since frequencies from 50 to 95 kHz are the less affected by background noise. Due to this narrow usable band, the processing gain keeps low if reasonable bit rates have to be achieved [43].

The requirement for higher data rates implies that the symbol duration is reduced. When that symbol is transmitted through a multipath channel, different copies of the same symbol arrive during a certain period. These copies can affect several symbols causing high inter-symbol interference (ISI), and in consequence complicated equalizers become necessary. In contrast, if we split the data stream in N_c different parallel sub-streams with lower data rates (N_c/T_d), these symbols will be much less affected by the ISI. Splitting the main stream implies that different parallel transmissions must be later performed. This was the initial motivation for MC modulation. Since the A band transfer function selectivity can be neglected, the MCM robustness against the frequency selectivity is exploited if focusing on the background noise. On the other hand, MCM robustness against narrowband interferers is a great benefit, since the destruction of one or several subcarriers can be recovered if the data has been properly coded. In a special type of MC modulation, OFDM, the different subcarriers overlap themselves reducing the required bandwidth (Figure 20) [16][18][19].

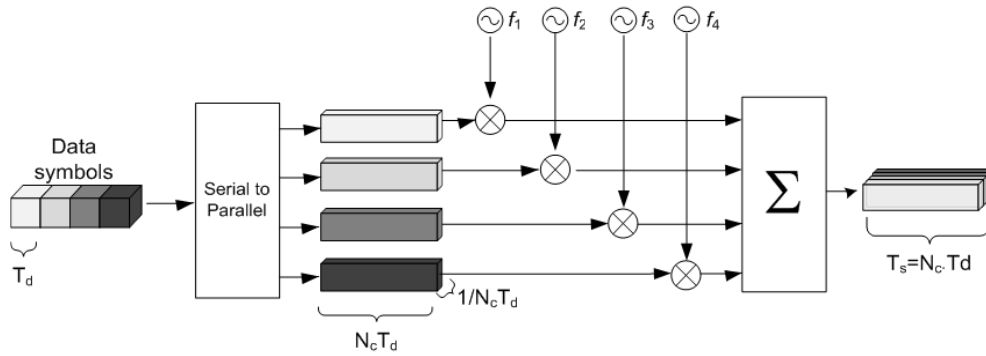


Figure 20 OFDM modulation scheme

Orthogonality between sub-streams can be assured by choosing subcarriers with an integer number of cycles within the symbol duration. If the minimum spacing between subcarriers becomes the inverse of the symbol duration, the highest spectral efficiency is obtained. The N_c data symbols transmitted during T_d are referred as an OFDM symbol, thus the OFDM symbol rate is $1/T_s = N_c/T_d$, where T_s is the OFDM symbol duration. An efficient digital implementation of the OFDM is accomplished by the Fast Fourier Transform (FFT) [18]. Moreover, the ISI can be completely avoided (if needed) if a guard interval is added at the beginning of each symbol [16].

3.3. MANUFACTURER SOLUTIONS

To the best of the author knowledge, there are five main integrated circuit manufacturers involved on AMR EN50065 compliant systems. These are the following:

- Echelon
- AMIS
- STMicroelectronics
- Yitran
- Adaptive Networks

The PL-3120, PL-3150 and PL-3170 from Echelon achieve 3600 bps of gross bit rate by means of a BPSK signaling with two selectable carrier frequencies. The AMIS-30585 uses a FSK variant called Spread-FSK (S-FSK). This modulation consists on a 10 kHz separated FSK tones. If any of these subcarriers is masked by interference, the system can keep working with the remaining subcarrier considering it as an ASK signal. With a programmable carrier frequency, it delivers 1200 bps of gross bit rate. The ST7538 from STMicroelectronics uses FSK to transport data from 600 to 4800 gross bit rate. Moreover, the carrier frequency can be selected among 6 possible choices. The IT800 implements a proprietary solution from Yitran, named differential code shift keying (DCSK), working at 625 and 2500 bps. Adaptive Networks also has an EN50065 compliant chip called AN48, signaling at 4800 bps by means of a SS like signal. It can be said that Yitran and Adaptive Networks are the only schemes that offer real frequency diversity. Table 3 summarizes the different chip characteristics [45][46][47][48].


					
Modulation	BPSK	S-FSK	FSK	DCSK	SS
Frequency diversity	Dual carrier freqs.	FSK to ASK	No	Yes	Yes
Maximum gross bit rate [bps]	3600	1200	4800	2500	4800
Upper layer implementation	Yes	Yes	No	Yes	NA

Table 3 Main AMR PLC chip manufacturers

3.4. MULTICARRIER PROPOSAL FOR AMR SYSTEMS

Previous non-spread proposals provide almost no level of frequency diversity, making some long term channel events, e.g., narrowband interferences and impedance mismatches, a serious impairment for the reliability of the communication link. The SS based modulations increase the occupied bandwidth more than what is strictly necessary yielding to a great robustness in front of interference and other frequency selective effects.

From Table 3, one can deduce a reduced processing gain, taking into account the delivered bit rate and the available bandwidth, i.e., 84 kHz for the entire A band or 30 to 40 kHz if only the noiseless upper region is wanted to be used. Moreover, SS modulations offer no spectral granularity and, for this reason, SS modulation can be considered as an interference mitigation mechanism, instead of interference avoiding mechanism.

A more advanced solution that offers higher robustness in front of interferences, a great level of frequency diversity and flexibility is proposed, while reducing the receiver complexity.

As stated before, MCM are suitable when dealing with frequency selectivity and narrowband interferences. Since one can expect a highly interfered scenario (narrowband interferers and coupling of other communication equipment), MC schemes seem to be a good choice for AMR systems. The MC receiver, and specially the OFDM one, presents two critical points. These are the time and frequency synchronization stages. MCM are very sensitive to synchronization errors, so relatively complex receivers are needed [16].

The presented proposal (deeply explained in Appendix A.2) shows a low complexity MC scheme for medium rate AMR systems. In order to deploy an AMR network, the cost of the equipment on the customer premises and the added value services that the system provides are two key factors in its business case. If we focus on modulation issues, the synchronization procedures are the most critical points that affect the complexity and cost of the equipment. In this situation, it is mandatory to use the implicit time reference that the power line network offers. The mains voltage zero-crossings offer a reliable time reference while the symbol rate is reduced. We had two options in order to increase the data rate. On one hand, we can increase the modulation level and, on the other hand, we can transmit several low symbol rate parallel streams. The channel impairments claim for a robust mapping, thus, only one bit per symbol is transmitted and BPSK is used as a reliable modulation scheme. The zero-crossing jitter effects can be mitigated by means of employing a MC modulation and a CPs.

3.4.1. ZERO CROSSINGS AS A TIME REFERENCE

From [4], the zero-crossing events can be characterized as a Gaussian random process as can be seen in Table 4. When information is sent from the TS to the customer site, the data and the time reference propagate in the same direction. Otherwise, if data is sent from the customer modem to the TS, the data and time reference propagate in opposite directions. In this case, a distance dependent delay between the data and the time reference occurs. The uncertainty of the zero-crossings around the mean is up to $STD = 100 \mu s$ in the worst case. This variance will be used in the sequel.

Propagation speed $0.577 \cdot c_0$	
DOWNLINK	
Mean	0 μs
STD	30 to 100 μs
UPLINK	
Mean	11.55 μs / km
STD	30 to 100 μs

Table 4 Zero-crossing jitter parameters

3.4.2. SC-BPSK PERFORMANCE IN FRONT OF WINDOWING ERRORS: LEADING TO THE MC APPROACH

Let us begin considering a SC-BPSK signal in presence of AWGN. This binary modulation consists of two signaling squared pulses of duration T' and amplitude A and $-A$. If a time offset misalignment is supposed, namely t_{off} , the theoretical bit error probability (BER), i.e. the probability of error (p_e), for a given bit energy to noise spectral density ratio (E_b/N_0), where d is the t_{off} to T' ratio, is shown in Eq. (3.1) and in Figure 21.

$$p_{e,d,T'}(e) = 0.5 \cdot Q\left(\sqrt{\frac{2E_b}{N_0}}\right) + 0.5 \cdot Q\left(\sqrt{\frac{2E_b(1-2d)^2}{N_0}}\right) \quad (3.1)$$

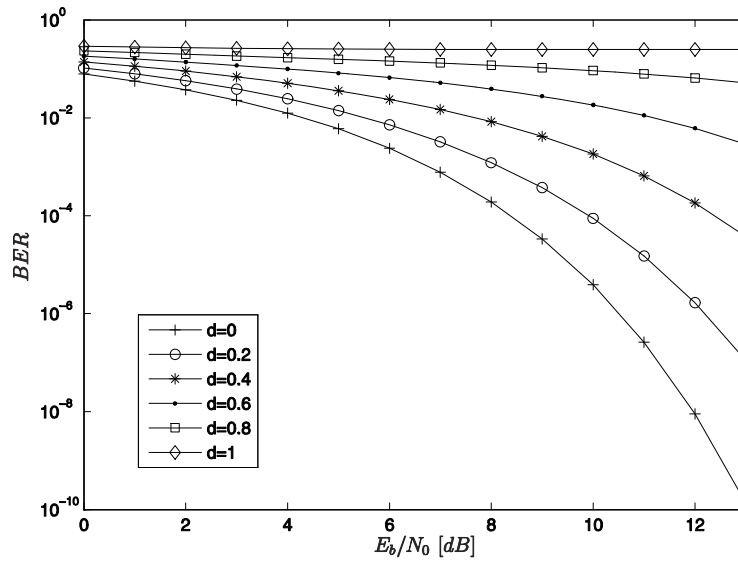


Figure 21 SC-BPSK performance in front of windowing errors

On one hand, as long as d increases, the performance is dramatically reduced due to inter-symbol interference (ISI), and, on the other hand, as the symbol rate is reduced, the ratio d decreases and the performance of the system increases. There is a trade-off between rate and quality. This problem can be overcome by splitting the high rate data stream into several low rate subchannels, leading to a MC approach.

3.4.3. MCM AND MAINS ZERO-CROSSING JITTER

By splitting the serial data stream into several low rate subchannels, a good d ratio can be achieved without decreasing the bitrate. Given the MC signal shown in Eq. (3.2) (where $\Pi\left(\frac{t}{T'}\right)$ is a squared pulse shaping waveform of amplitude 1 and duration T') and the zero mean Gaussian distribution of the mains zero-

crossing jitter, namely $p_j(jit)$, with $STD = 100 \mu s$, the performance of such signal affected by the windowing synchronization errors due to $p_j(jit)$ is shown in Eq. (3.3) and depicted in Figure 22.

$$s(t) = \Re e \left\{ \sum_{n=0}^{N_{SC}-1} b_n \cdot e^{j \cdot 2\pi(f+n \cdot m \cdot \Delta f)} \cdot \Pi\left(\frac{t}{T'}\right) \right\} \quad (3.2)$$

$$P_{e,T'}(e) = \int_{-\infty}^{\infty} P_j(t_{off}) \cdot P_{e, \frac{t_{off}}{T'}, T'}(e) \cdot dt_{off} \quad (3.3)$$

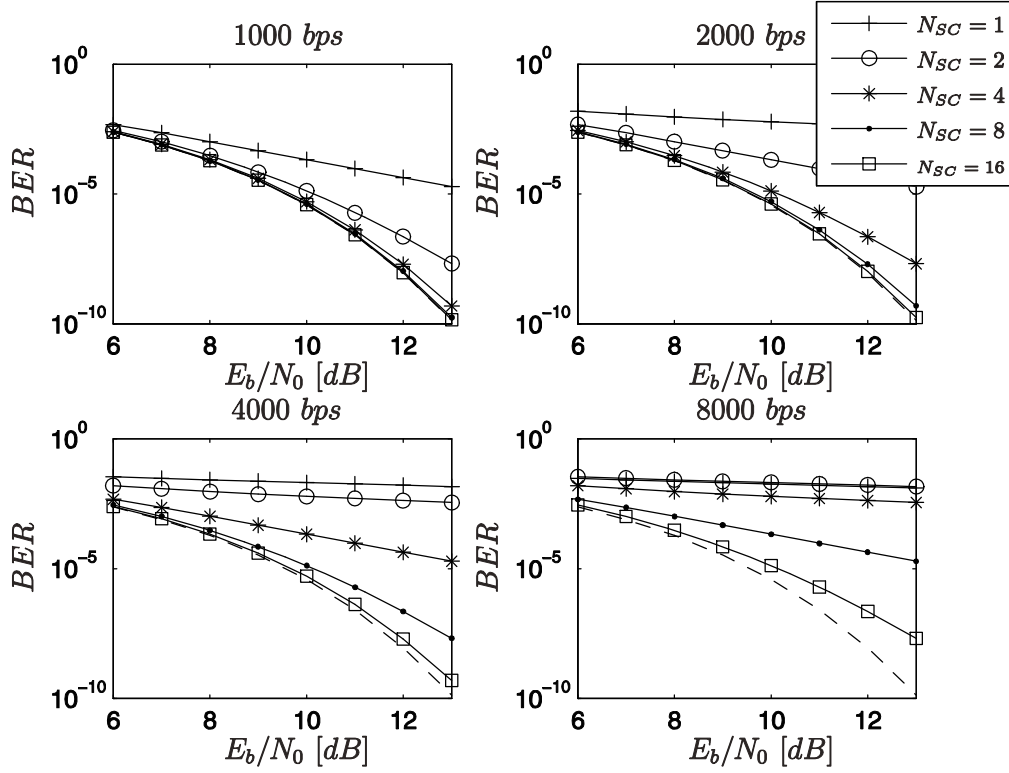


Figure 22 MC-BPSK performance in front mains zero-crossing jitter

Where b_n are the BPSK modulated symbols, N_{sc} the number of subchannels or subcarriers, $\Delta f = 1/T_s$ the minimum needed intercarrier spacing in order to keep the N_{sc} subcarriers orthogonal, $m \cdot \Delta f$ is the actual intercarrier separation and n is the subcarrier index, ranging from 0 to $N_{sc} - 1$. For reduced data rates, around 1000 bps, the splitting of the data into more than two subchannels has little effect in the improvement of the system performance. As long as the data rates increase, a higher number of subcarriers are required in order to maintain the BER low.

3.4.4. RESIDUAL INTER-SYMBOL INTERFERENCE: CYCLIC PREFIX AND POSTFIX

The superior performance of splitting the high rate single carrier signaling into several low rate MC subchannels has been shown. The longer the symbol is, the better d ratio, but the ISI between MC symbols is still present with a probability of $p_j(jit)$. In order to reduce, even more, the effect of the jitter; i.e. ISI and in a MC scenario, inter-carrier interference (ICI) too; we will add a cyclic prefix (CP^+) and a cyclic postfix (CP^-) at the beginning and at the end of each MC symbol respectively [16]. The objective of the insertion of these pre and postfixes is the cancellation of the ISI (this will keep the N_{sc} subcarriers orthogonal) as long as the $\pm d \cdot T'$ is less than the duration of the cyclic pre and postfix. Since being misaligned $+d \cdot T'$ and $-d \cdot T'$ is equiprobable, we will set the same duration to the prefix and postfix. We will refer to this duration with the ratio of CP_i to T_s ratio, namely c , where CP_i is the CP^+ and CP^- length.

In order to evaluate the impact on the performance of using the pre and postfix, we will redefine the distribution of probability of the jitter ($p'_j(jit)$) as can be seen in Eq. (3.4). Using this new jitter probability distribution function, the probability of error as a function of c , d and T_s is shown in Eq. (3.5) and depicted in Figure 23 for an E_b/N_0 of 12dB.

$$p'_j(jit) = \begin{cases} \int_{-CP_l}^{+CP_l} p_j(j) dj & \text{for } jit = 0 \\ 0 & \text{for } 0 < |jit| < CP_l \\ p_j(jit) & \text{for others} \end{cases} \quad (3.4)$$

$$p_{e,c,T'}(e) = \int_{-\infty}^{\infty} p'_j(t_{off}) \cdot p_{e,c,\frac{t_{off}}{T'},T'}(e) \cdot dt_{off} \quad (3.5)$$

where

$$p_{e,c,d,T'}(e) = 0.5 \cdot Q \left(\sqrt{\frac{2E_b \left(1 - \frac{2c}{N_{SC}}\right)^2}{N_0}} \right) + 0.5 \cdot Q \left(\sqrt{\frac{2E_b \left(1 - \frac{c}{N_{SC}} - 2\frac{d-c}{N_{SC}}\right)^2}{N_0}} \right) \quad (3.6)$$

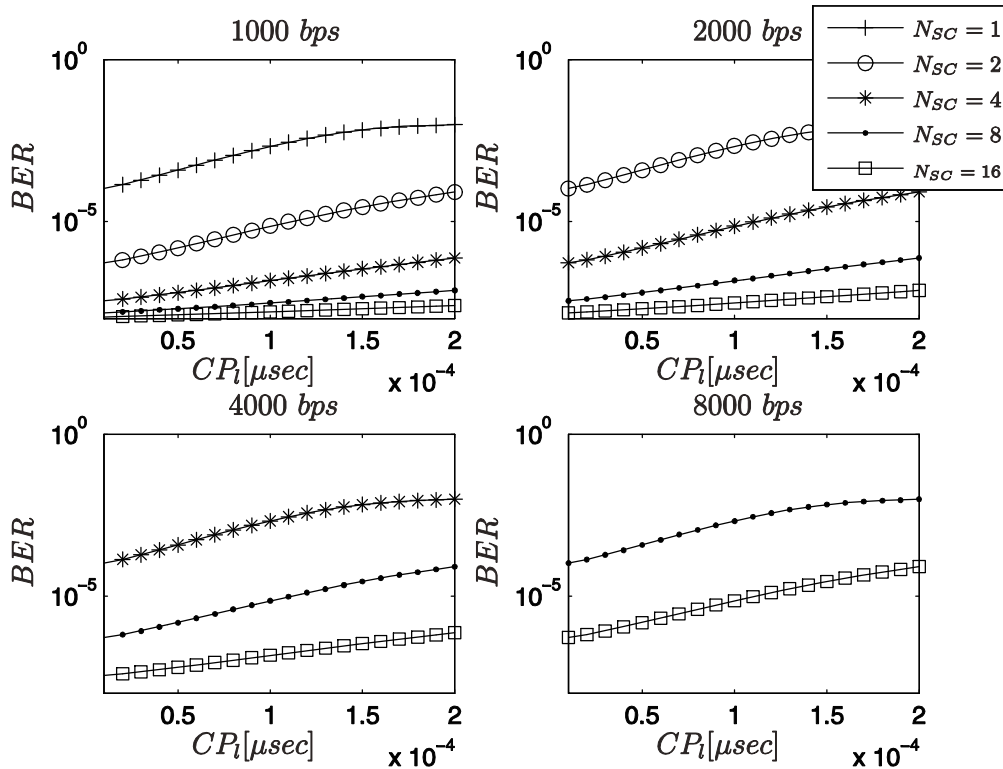


Figure 23 MC system performance for various CP lengths

From Eq. (3.6), one can expect a decrease of the system performance, since the use of cyclic pre and postfixes implies a waste of power that will not be used for signal detection. Figure 23 depicts this situation. For reduced data rates, around 1kbps, and 8 or 16 subcarriers, the performance degradation due to the reduction of the power available for detection is almost negligible. Obviously, as the data rates increase while the number of subcarriers remains constant, that waste of power notably reduces the performance of the system.

Although it seems that it is not worth to employ a cyclic prefix, since far away from improving the performance, it is reduced; the advantage of using these CPs is that we are preventing ICI from occur. In a MC environment, when ISI occurs, not only the degradation shown in Figure 22 happens, moreover, the orthogonality among subcarriers is destroyed, causing a higher degradation that the one caused by ISI in a single carrier situation. The use of the cyclic prefix will allow us to keep the subcarriers orthogonal when time misalignment occurs, preventing ISI from causing ICI [16].

In a LV-PLC channel, only different frequencies between the transmitter and the receiver clocks can be expected to be ICI sources. A study of the frequency mismatch effect between clocks will be fulfilled.

3.4.5. FREQUENCY OFFSET AND SYSTEM PERFORMANCE

Apart from the advantages above mentioned, MC modulations are very sensitive to synchronization errors. The frequency offset correction between transmitter and receiver is a key step in the demodulation process. In our scenario, this frequency offset is caused by a frequency mismatch between the transmitter and the receiver clocks [16].

If the frequency offset is not corrected before the MC demodulation, two problems arise:

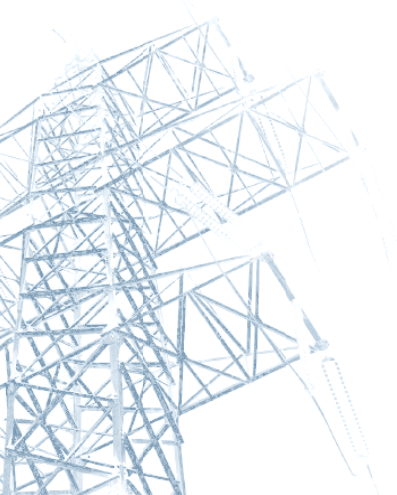
1. We are not sampling the subcarriers in the optimum point, so a decrease of the available power that will be used for detection occurs.
2. This deviation from the optimal sampling point will yield to the undesirable sampling of the others subcarriers causing ICI.

The spectral representation of a MC signal can be expressed as Eq. (3.7), where SC_n is the n -subcarrier spectrum. Let's see the performance degradation caused by a frequency offset of ζ_f Hz between the transmitter and receiver clocks (see Figure 24).

$$S(f) = \sum_{n=0}^{N_{SC}-1} b_n \cdot SC_n(f, m, T') \quad (3.7)$$

where

$$SC_n(f, m, T') = \frac{\text{sinc}\left(\frac{f + n \cdot m \cdot \Delta f}{\Delta f}\right)}{\Delta f}$$



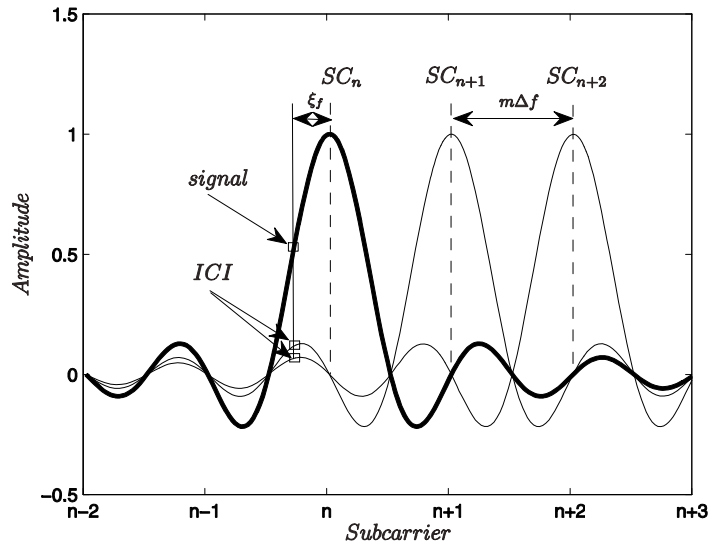


Figure 24 MCM spectrum

Several studies approach this ICI as a noisy Gaussian process applying the central limit theorem [16]. This is only applicable when the number of subcarriers is high enough. In this work, an exact calculation is derived, useful for a low number of subcarriers (Appendix A.2).

The relative frequency offset to the intercarrier spacing can be defined as $\nu = \zeta_f / \Delta f$. For a given ζ_f , it is interesting to choose a high enough Δf in order to keep ν as low as possible. If the SC_n are too narrow, the frequency offset will cause a low amplitude sampling of that SC_n . Otherwise, if we set SC_n wide enough, for a fixed ζ_f , we will sample more signal level. From Eq. (3.7) and Figure 23, a reasonable trade-off between SC_n width and robustness against the jitter can be a T' of 1 ms. This symbol rate ($R_s = 1/T' = 1$ kbps), can be delivered with several values of N_{sc} . The higher N_{sc} , the more throughput we will get, but more interferers we will have in case of $\zeta_f \neq 0$.

For this first proposal, we will choose $N_{sc} = 8$ and $R_s = 8000$ bps, as well as a cyclic prefix length of $200 \mu s$ and a postfix of the same length, giving in a useful symbol time of $T_U = 600 \mu s$.

As mentioned before, ICI is caused by a mismatch between the transmitter and the receiver clock frequencies. Let us fix what is the ζ_f we can deal with. In order to maintaining the costs low, we have to choose a low cost standard crystal as a reference. These range of crystals typically offer a calibration tolerance of ± 30 ppm and a temperature stability of ± 50 ppm. Taking into account that both link sites are located close to each other, we will suppose a maximum temperature difference of $25^\circ C$. For an average carrier frequency of 100 kHz, in the worst case we can receive 100 kHz ± 253 Hz, i.e. a $\zeta_f = 253$ Hz.

In order to avoid the introduced ICI, we will spread the subcarriers $m \cdot \Delta f$ Hz. Figure 25 depicts the effect on the system performance of spreading the subcarrier more than what is strictly necessary. The dashed line represents the ICI-free scenario. For $m = 1$, the performance dramatically decreases to an unacceptable levels, for $m = 4$, it approaches the ideal dashed line, occupying a bandwidth of 53.3 KHz. For $m > 4$, the performance is slightly improved. So, $m = 4$ seems to be a good trade-off between occupied bandwidth and robustness against clock frequency offsets.

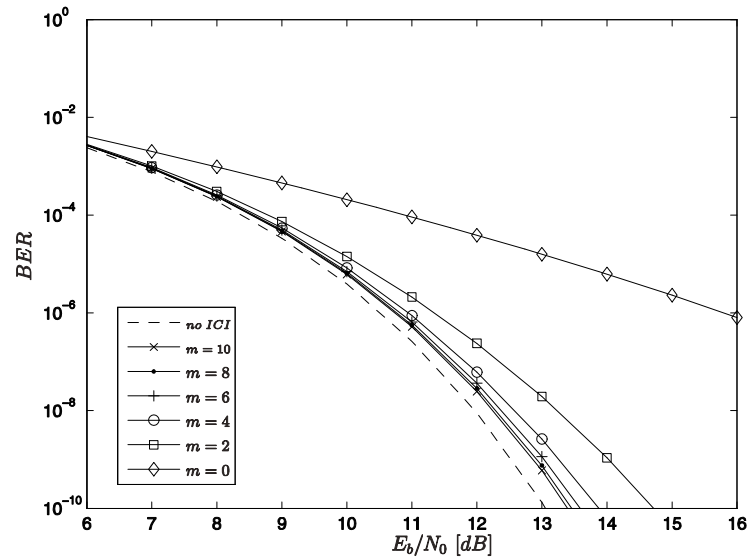


Figure 25 System performance for a frequency offset of 253 Hz, 8 subcarriers at 8 kbps

3.4.6. PHASE RECOVERY

The last synchronization stage to be faced is the phase detection and compensation in order to correctly detect the BPSK symbols. In our approach, the differential version of the BPSK is proposed instead of the coherent one. The DBPSK receiver is less complex and offers similar performance than its coherent implementation. For $E_b/N_0 > 10$ dB, the BPSK outperforms the DBPSK only by approximately 1 dB [42].

All the discussion made up to this point is valid for a DBPSK approach by shifting the performance curves 1 dB.

3.5. CONCLUSIONS

As an initial approach, the proposed system is shown in Table 5.

Parameter	Value
Symbol time	1 ms
Cyclic prefix length	200 μ s
Cyclic postfix length	200 μ s
Useful symbol time	600 μ s
Number of subcarriers	8
Mapping	DBPSK
Bit rate	8000 bps
Minimum subcarrier spacing	1.6 kHz
Actual subcarrier spacing	6.6 kHz
Occupied bandwidth	53.3 kHz
Carrier frequency	41.6 kHz

Table 5 Proposed system characteristics

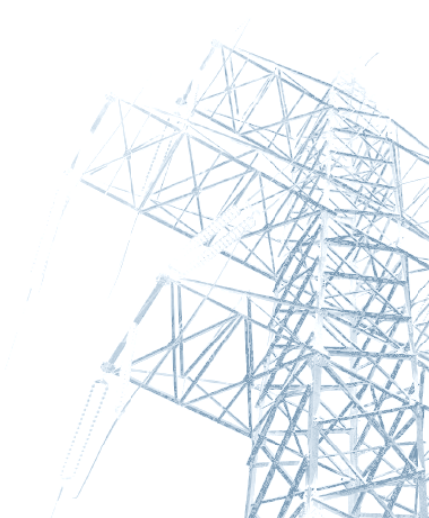
The drawback of this kind of modulation is its sensitivity to ICI. In this scenario, ICI is caused by ISI and by the frequency difference between system clocks. The first source of ICI is attenuated by means of the CPs. There is still a residual probability of ISI, since the cyclic prefix and postfix lengths are limited (Appendix A.2). The second source of ICI, far from being corrected, is supported. The separation of the subcarriers along the available frequency range more than what is strictly necessary reduces the effect of the interfering subcarriers into the subcarrier of interest. Coherent MC modulations need a channel estimation and equalization stages before signal demapping and detection. This process involves an added complexity to

the system, so, the differential version of the BPSK will avoid that cost with a low decrease of the system performance [15].

Current manufacturer solutions, as well as existing proposals in the literature, offer limited diversity (in terms of noise scenario and interference robustness) or, on the other hand, they are too complex to be implemented at a large scale with reduced costs. Regarding Endesa Spanish customers only, there are more than eleven million meters that will be replaced by AMR devices, so, in this scenario, the cost of the equipment is a key factor in the AMR system business case.

Moreover, added value services as dynamic billing, load balancing and fraud detection are also key factors when deciding the implementation of an entire AMR system. In order to cover the EUs new applications, an increase of current systems performance is demanded, while keeping the cost of the modem low.

The zero-crossing synchronized MCM based physical layer seems to be the current trend in robust AMR modem design. MCM offer great robustness against noise diversity as well as a high level of flexibility when dealing with such noise scenario and interferences. The proposed system offers such performance with a notably reduced receiver complexity. Recent studies regarding zero-crossing statistics have revealed that the jitter variance is lower than the one supposed during this design, so, considering the presented values in [85], the efficiency of the system regarding the cyclic prefix can be increased.



CHAPTER 4

4. MEDIUM VOLTAGE CHANNEL MEASUREMENTS AND ITS DETERMINISTIC-STATISTICAL MODEL

After the Endesa Distribución Eléctrica S.L. project, Endesa Network Factory S.L., another company from Endesa S.A., started a new one involving the MV and HV power grid. Before going to the HV network, a study of the MV power grid, specifically in urban underground networks, was carried out. This study began by measuring and characterizing both the channel transfer function and noise scenario. The former measurements, in addition with others done in the laboratory, yielded to the needed raw material to build a MV ring transfer function deterministic model.

4.1. INTRODUCTION

In conjunction with the LV network, the MV network comprises the distribution stage of the electric power grid. Located after the last step-down ES, and with typical levels from 6 to 25 kV, the MV network feeds directly large commercial or industrial consumers and domestic and small commercial consumers through several TS.

In urban areas, the MV network is fully underground while in rural areas, both overhead and underground topologies can be found. This work will focus on underground urban ring shaped networks. The Ring topology, consisting of two MV feeders departing from the ES, shares a common point named the border of the ring. This border is an open circuit between the two radial MV lines. This border can be moved in order to limit the impact of a failure into the network, minimizing the length of the segment (and the number of TS) affected by the failure (Figure 11) [22][50]. The average number of TS per MV ring ranges from 4 to 30 and each TS is located from 150 to 400 meters away from the next one in urban areas [50].

A key point in a physical layer design process is the channel model. If properly implemented, the channel model will allow the correct modulation and access methods design. Before modeling, channel characterization has to be carried out [51][52].

4.2. CHARACTERIZATION AND MODELING APPROACHES

Regarding channel characterization or definition, two different approaches can be followed:

- Behavioral. This is a top-down strategy, where the statistical characterization of the system is based on exhaustive channel measurements. It is not straightforward to define reference models, since even more exhaustive measurements are needed to cover power networks worldwide casuistic. This is the followed approach when dealing with random channel effects, such as the noise scenario [65] or when the channel topology is extremely complex, e.g., LV networks [51].
- Structural. This is a bottom-up strategy, where physical parameter estimation is more intuitive and derived from single measurements of the power line network elements. Model adaptation to power grid features worldwide is easier. Focusing MV channel characterization, some transmission line model based works can be found [63][64][61][79][80].

Regarding channel modeling, two analogous approaches can be followed too:

- Stochastic. Derived from behavioral characterization, these channels models simulate channel conditions based on statistics. As stated, they are typically employed when modeling noise or complex topologies [24][25]. Very usual in LV network modeling: [53][54][58].
- Deterministic. Derived from structural measurements and their structural devices definition, deterministic models are restricted to simulate the modeled structure, without random elements.

Some examples of such modeling technique can be found in [61] regarding MV and in [56][57] regarding LV.

This work measures structural parameters of a MV ring and their devices in order to deterministically model their behavior and then, based on statistic records of European MV networks, add the parameters that will make the model valid for several regions [59][60]. Then, a behavioral characterization of the noise scenario, regarding both background and impulse events, will be given (Appendix A.3 and Appendix A.5).

4.3. MEASUREMENTS

The aim of this work is to provide a set of measurements in order to get the needed physical knowledge to define a proper deterministic-statistical model for MV networks. The measurements described hereafter have been done in a 324 meters link in Barcelona, Spain, between the Endesa substations BA07460 and BA07155 (Figure 26).



Figure 26 Endesa BA07155 and BA07460 TSs

In this work, different measurements will be carried out in order to characterize the following urban underground MV channel effects:

- Input impedance. Mainly affected by:
 - Characteristic impedance of the MV cable.
 - Connected feeder's loads.
- Noise scenario.
 - Background colored noise: In MV networks, this noise is mainly caused by leakage or discharge events, power converters, transformer non idealities... As well as in HV networks, stationary low-power periodical and synchronous with the mains impulse events can also be considered background noise. These kinds of impulses are caused by discharges on insulators and other ES or TS devices.
 - Narrowband noise: Narrowband interferences such a coupled broadcast emissions or other communications equipment are considered background noise.

- Impulse events: The main causes of this noise type are network switching transients (isolator switching or breaker operation), lightening and other discharging events.
- Attenuation and frequency selectivity. Caused by power dissipation and reflections in the grid or coupling devices. These two effects are included in the channel transfer function.

This set of measurements consists of:

1. Field measurements and results:
 - a. Attenuation characteristics.
 - b. Time spread and frequency spread.
 - c. Background noise.
 - d. Impulsive interferences.
 - e. Reflection coefficient.
2. Laboratory measurements and results:
 - a. MV cable S parameters characterization.
 - b. MV coupler S parameters characterization.
3. Joint results:
 - a. Input Impedance.

See Appendix A.3 for a measurement set-up description and deepest explanation of the measurements.

4.3.1. FIELD MEASUREMENTS

The following measurements have been done in the previously presented link.

ATTENUATION CHARACTERISTICS

In Figure 27, the attenuation of the link under study is depicted. The dashed line shows the overall link attenuation, i.e., the attenuation due to the cable losses, the reflection and transmission capabilities of the coupler and the input impedance and parallel loads connected to that link. As stated, since there are more parameters than the intrinsic cable attenuation, the continuous line depicts an approximation of the attenuation per hundred meter, showing similar values like the ones in Reference [28].

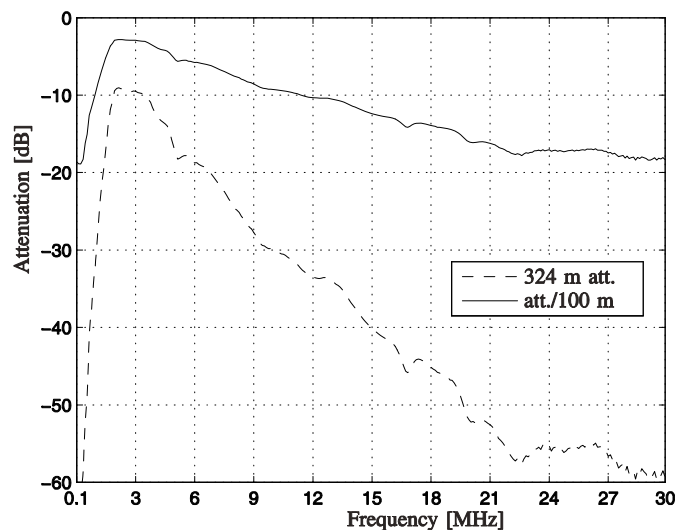


Figure 27 MV ring segment attenuation

The time behavior of this characteristic is notably constant, with negligible variations over time. The attenuation characteristic band-pass shape is mainly due, on one hand, to the 1 nF coupler capacitor and to

the effect of the embedded impedance matching network [27], and, on the other, to the MV cable attenuation.

TIME SPREAD AND FREQUENCY SPREAD

By means of pseudo-noise (PN) based channel sounding, the channel delay and Doppler spread values will be given.

Equation (4.1) shows the transmitted signal, $s(t)$, consisting on a modulated maximal length sequence (m-sequence) train with center frequency $f_c = 2.5$ MHz, located at the pass band center of the attenuation characteristic.

$$s(t) = \Re \left\{ \sum_{n=0}^{N_{sq}-1} s_{PN}(t-nT) e^{j2\pi f_c t} \right\} \quad (4.1)$$

where

$$s_{PN}(t-nT) = \sum_{i=0}^{N_c-1} b_i \cdot p \left(t - i \frac{T}{N_c} - nT \right)$$

Where $s_{PN}(t)$ is a PN sequence of length N_c chips that have been interpolated by a pulse shaping filter $p(t)$, $b_i \in \{-1, 1\}$ are the sequence chips, N_{sq} is the number of m-sequences per burst, T is the sequence period, T_c is the chip period and ΔT_s is the sounding or burst period. This technique allows an unambiguous sounding when the channel has a impulse response, $h(\tau)$, shorter than T , with a time resolution of T_c , allowing a maximum detectable Doppler of $1/2T$ with an accuracy of $1/\Delta T_s$. Table 6 shows the sounding parameters.

Parameter	Value
Sequence type	m-sequence
Number of chips	511
Chip period	1 μ s
Sequence period	511 μ s
Number of sequences per burst	200
Pulse shaping filter	Root raised Cosine ($\alpha = 0.65$)
Occupied bandwidth	1.65 MHz
Center frequency	2.5 MHz
Maximum detectable delay	511 μ s
Delay resolution	1 μ s
Maximum detectable Doppler	978 Hz
Doppler resolution	9.7 Hz

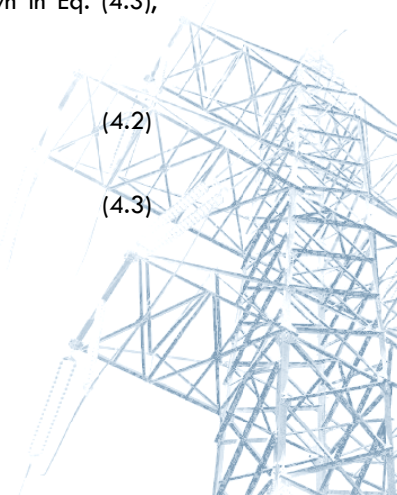
Table 6 MV PN sounding parameters

After downconversion, the base-band received m-sequence train, $r_{PN}(t)$, is correlated with a local PN sequence replica $s_{IPN}(t)$, as shown in Eq. (4.2). If N_{ov} is the oversampling factor, i.e., the number of samples per chip; the discretized channel impulse response matrix $h[n, \eta]$ can be obtained as shown in Eq. (4.3), where n and η are the time and delay indexes respectively.

$$R_{r_{PN}, s_{IPN}}(t) = \int_0^T r_{PN}(t+\tau) s_{IPN}(\tau) d\tau \quad (4.2)$$

$$h[n, \eta] = R_{r_{PN}, s_{IPN}} \left(\eta \frac{T}{N_c N_{ov}} + nT \right) \quad (4.3)$$

where



$$n \in \mathbb{N} \quad n \in [0, N_{sq} - 1]$$

$$\eta \in \mathbb{N} \quad \eta \in [0, N_c N_{ov} - 1]$$

Figure 28 shows the channel delay power profile, revealing the energy spread in time domain. This spreading, most probably caused by the coupling equipment, presents a spreading of $1\mu\text{s}$ and $7\mu\text{s}$ at 10 and at 40 dB respectively.

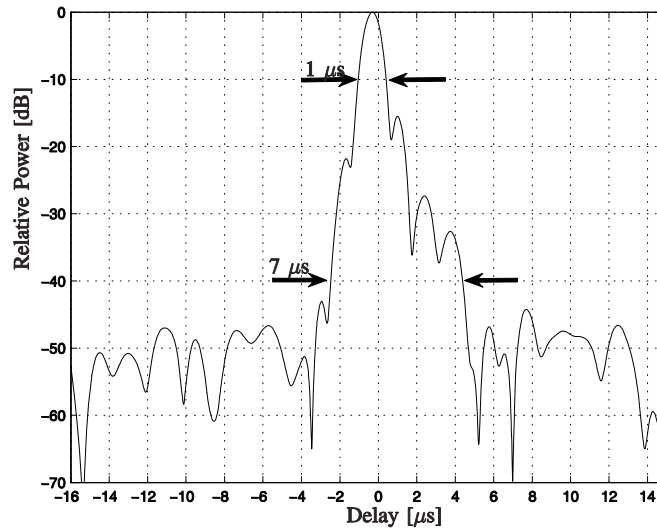


Figure 28 MV ring segment delay power profile

BACKGROUND NOISE

One of the most characteristic aspects of PLC channels is their noise scenario. Simplifying the typical noise scenario defined in [24], two kinds of noise analysis will be carried out:

- **Background Noise.** Including several low power spectral density (PSD) noise sources, narrowband interferences (mostly very slow variant sinusoidal signals) and low power periodic impulsive noise: some impulsive events also remain stationary, so, in this work, impulses with a continuous repetition and with a peak power 6 dB or less than the background noise mean power will be considered background noise too.
- **Impulsive Interferences.** Those impulses not considered background noise, i.e., impulses with a peak power more than 6 dB than the background noise mean power.

Figure 29 depicts the mean PSD and the standard deviation (STD) in the frequency domain. These statistics reveal a highly colored background noise until 10 MHz, and from that point on, the delta-like spectrum is related to low-power continuous impulsive events. The colored behavior, due to the summation of several noise sources, remains at low frequencies, where the propagation from those sources to the measurement point is possible. The maximum variability has been observed in that frequency range, while in the highest ranges, only minor changes happened.

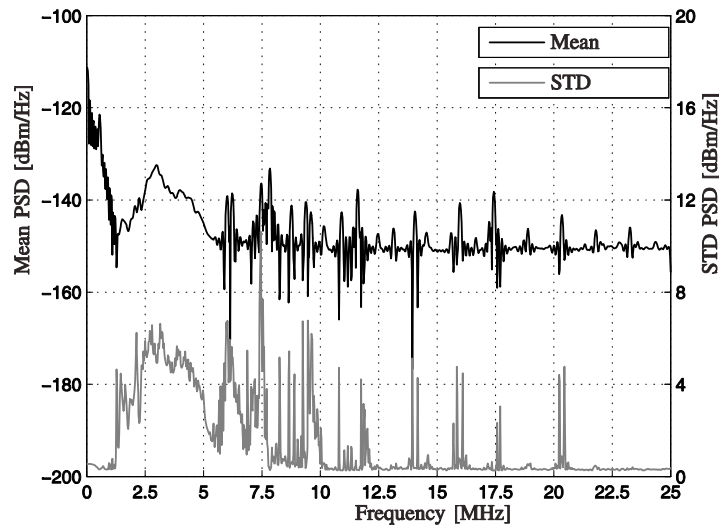


Figure 29 MV ring segment background noise statistics

IMPULSIVE INTERFERENCES

While some noisy events remain stationary during time with a relatively low power, several impulsive interferences are characterized by their high amplitude. During 4 days, more than 18 minutes sampled at 20 Msps have been processed to extract the following statistics. That observation time yields to 7,426,304 analyzed impulses.

The horizontal parameters, i.e., random variables (RV), that typically characterize these impulse events [24] are the impulse width t_w , and the interarrival time t_{iat} that is, the time between the rising of the impulse and the end of the same, and the time between two consecutive pulse risings, respectively. Moreover, impulse interferences will be also characterized by two vertical parameters, i.e., impulse peak power p_{pk} and impulse average power p_{av} (Figure 30).

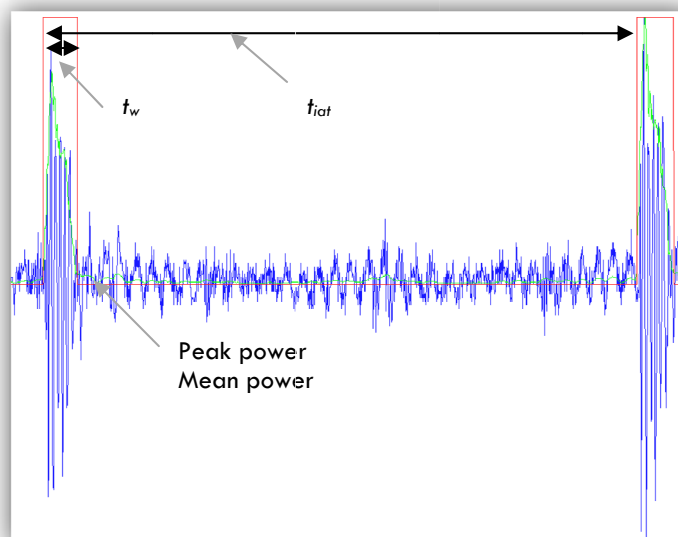


Figure 30 Impulsive waveform parameters

Figure 31 and Figure 32 depict the probability density function (PDF) and complementary cumulative density function (CCDF) for the time and power related RVs, respectively.

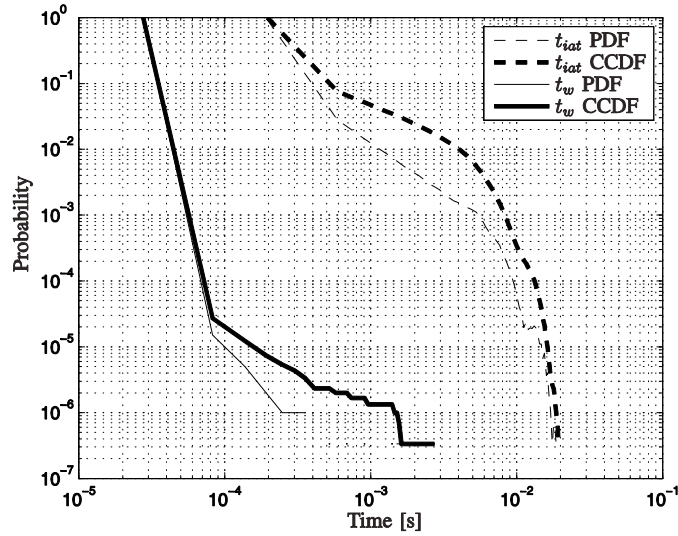


Figure 31 MV ring segment inter-arrival and width times statistics

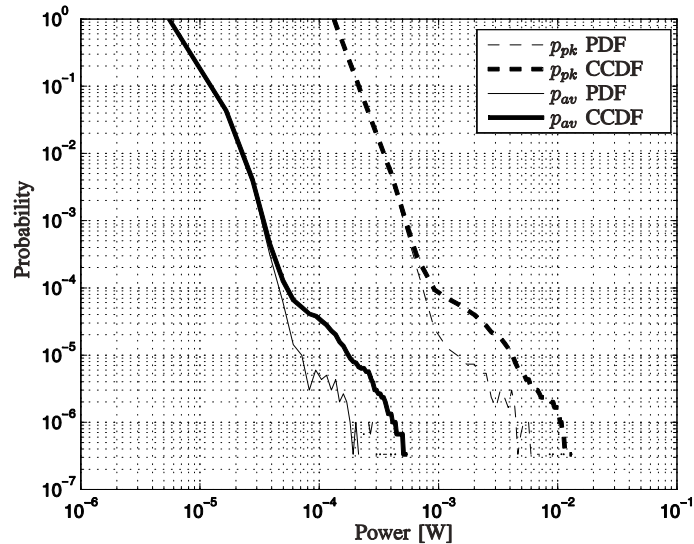


Figure 32 MV ring segment peak and average power statistics

On one hand, impulses with durations less than 0.1 ms have an occurrence probability of $1 \cdot 10^{-5}$, showing that almost all impulse durations are in the range of tens of microseconds. On the other, interarrival times of milliseconds, are quite usual ($>10^{-1}$), undisturbed intervals over tens of milliseconds can arise with a probability of 10^{-3} . Figure 32 depicts that p_{pk} CCDF is a shifted version of p_{av} CCDF, showing that almost all impulses have the same shape or damping factor.

REFLECTION COEFFICIENT

Input impedance, specially when dealing with power line networks, is a key characteristic of the transmission channel, since it is different for different topologies and rules the power that the transmission and reception devices will be able to inject and recover from the network, respectively.

By means of the microwave network analyzer (MWNA), the MV channel reflection coefficient, measured at the coupler equipment side will be used for the network input impedance extraction, where the coupler behavior will be compensated in order to get the actual channel reflection coefficient and input impedance, thus.

4.3.2. LABORATORY MEASUREMENTS

The following measurements have been carried out in order to characterize, by means of S parameters, the cable and the coupler.

MV CABLE S PARAMETERS CHARACTERIZATION

In urban areas, Endesa is now mainly deploying 18/30 kV unipolar underground cable, with triple extruded aluminium core and cross linked polyethylene (XLPE) dielectric, compiling the rules EN-50267-2-1, IEC-60502.2 and Endesa proprietary rules DND001 and SND013. The objective of this measurement is to gain knowledge of that MV cable propagation constant γ , Eq. (4.4), and characteristic impedance Z_0 .

$$\gamma = \alpha + j\beta \quad (4.4)$$

$$\beta = 2\pi f / c \quad (4.5)$$

In

$$V(z) = V^+ e^{-\gamma z} + V^- e^{\gamma z}$$

Where $V(z)$ is the progressive voltage wave $V^+ e^{-\gamma z}$ plus the regressive voltage wave $V^- e^{\gamma z}$ in their phasorial representation.

The extraction of these cable characteristics has been carried out as follows:

1. Precise cable length measure, in our case 10,51 m.
2. Manufacture of the cable to NA discontinuity connection. The MV cable to the NA measurement port connections (Figure 33) need an ad-hoc transition manufacture. These discontinuities involve geometrical changes in the cable structure, modifying its behavior, specially, at high frequencies.

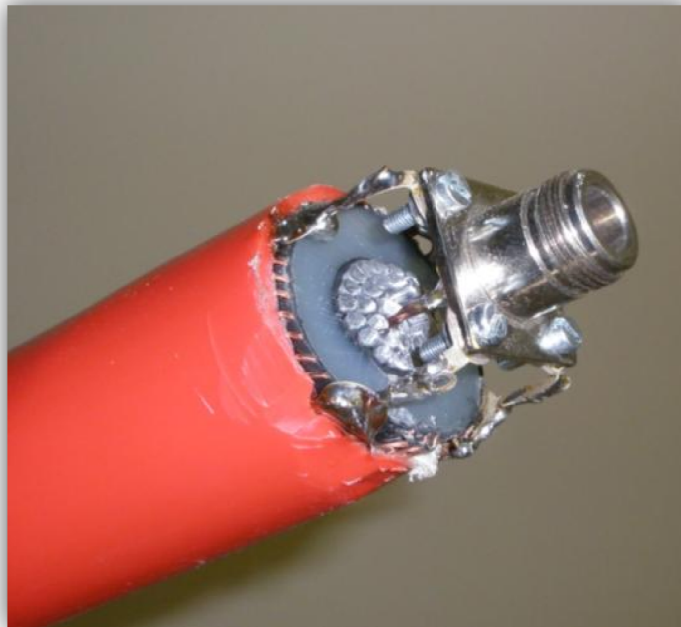


Figure 33 MV cable to N connector

3. S parameters measurement.

4. Transitional connection modeling. In order to extract the discontinuity effect from the previous measurement, at both cable ends, the transition is modeled by a serial anticon and a parallel anticon, i.e., a coil and a capacitor with negative inductance and capacitance, respectively. When those discontinuity effects are extracted, the resulting S matrix will describe the behavior of the MV cable only, without the effect of the transitional connection.
5. Compensation and deembedding of the discontinuity connection geometrical change by means of gradient based optimization. An impedance matched transmission line has a near zero reflection parameters. With the target of achieving such reflection values, an optimization of the above mentioned anticon and anticon, as well as the unknown characteristic impedance Z_0 is carried out, obtaining a cable reflection coefficient less than -25 dB from 10 kHz to 500 MHz. Figure 34 shows the cable S parameters after the optimization for a 10 m length segment. At this point, the cable discontinuity parasite behavior can be considered compensated and the actual cable parameters extracted. Equation, shows the third order polynomial that fits the transmission parameter] with a root mean square error less than 0.1.

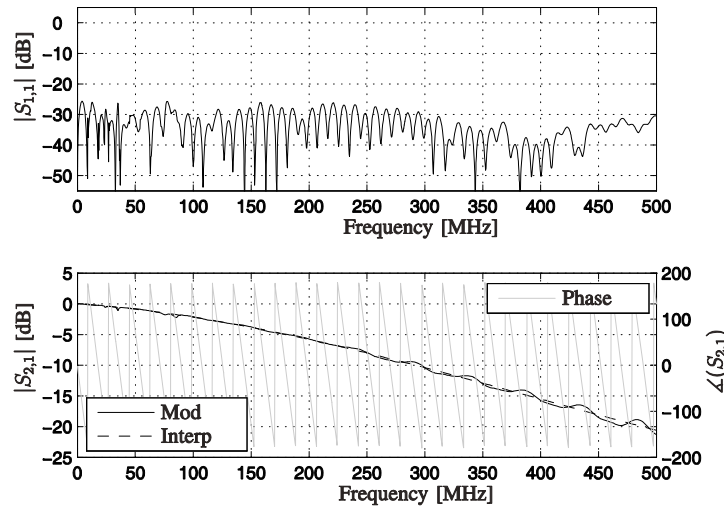


Figure 34 MV cable S parameters

As can be seen in Figure 34, the reflection coefficient has been minimized by means of the step gradient descent algorithm, achieving an adaptation better than -25 dB in the reflection coefficient, in the whole frequency range. This minimum values correspond to the cable characteristic impedance shown in Eq. (4.6).

$$Z_0(f[\text{MHz}]) = 24.53 + 3.22 \cdot 10^{-2} \cdot f \quad [\Omega] \quad (4.6)$$

The attenuation coefficient α is directly extracted from the transmission coefficient. That curve can be closely approximated by a 3rd order polynomial fitting shown in Eq. (4.7) (Figure 34).

$$\alpha(f[\text{MHz}]) = 8.1 \cdot 10^{-8} \cdot f^3 - 9.7 \cdot 10^{-10} \cdot f^2 - 13 \cdot 10^{-2} \cdot f - 0.029 \quad [\text{dB}/10\text{m}] \quad (4.7)$$

Finally, from the transmission coefficient phase rotation in the 500 MHz frequency range, and taking into account the cable length (Eq. (4.5)), the propagation velocity can be known as shown in Eq. (4.8), where l and φ are the cable length and phase rotation respectively.

$$c = \frac{2\pi \cdot f \cdot l}{\varphi} = 1.9 \cdot 10^8 \quad [\text{m/s}] \quad (4.8)$$

Figure 35 summarizes the extracted MV cable parameters, yielding to the complete definition of the characteristic impedance and propagation constant, i.e., attenuation and phase coefficients.

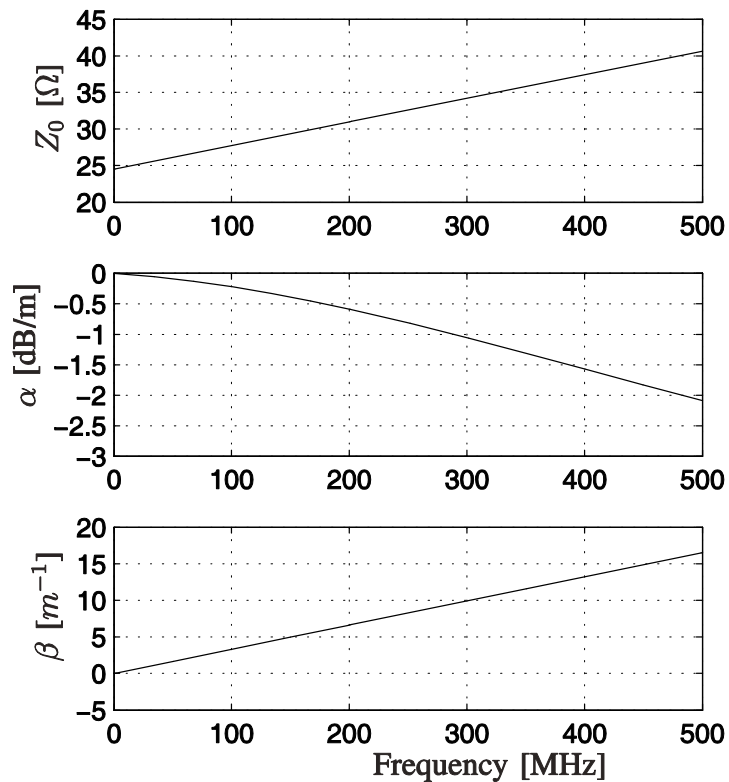
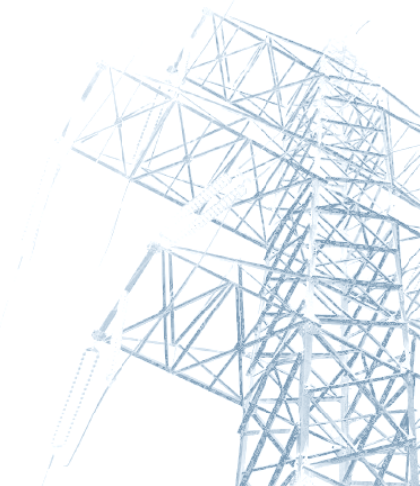


Figure 35 Extracted MV cable parameters

MV COUPLER S PARAMETERS CHARACTERIZATION

The PLCoupling / DIMAT CAMT-1 capacitive coupler is intended to adapt a communications equipment impedance of 50 Ω to an expected line access impedance of 20 Ω . The S parameters are extracted and used in the input impedance measurement and also in order to know how different from the expected line access impedance affect coupler performance. It has been found by simulation that if MV channel access impedance is different from the expected, the coupler performance varies, as shown in Figure 36, where transmission and reflection performances are depicted for an access impedance of 10, 20 and 30 Ω .



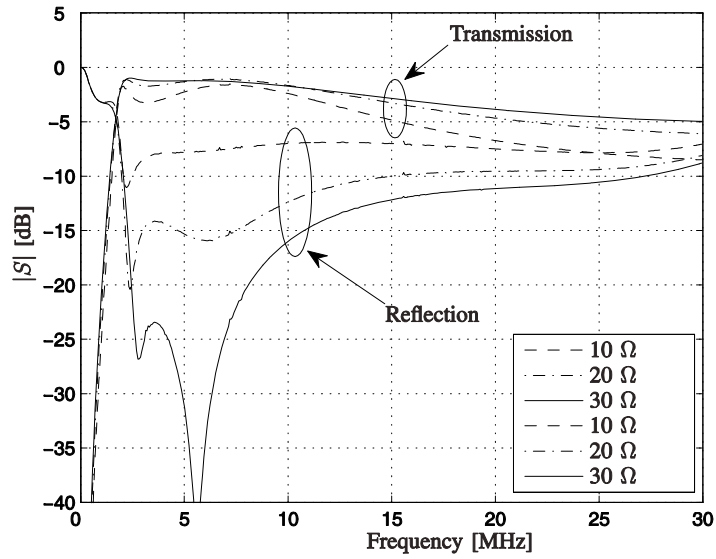


Figure 36 MV coupler performance variations

4.3.3. JOINT MEASUREMENT: INPUT IMPEDANCE

Finally, by means of the coupler S parameters characterization as well as the measured channel reflection coefficient, the input impedance deduction will be fulfilled.

Being the coupler S parameters, namely S_c (Figure 37), and the measured channel reflection coefficient, namely Γ_{IN} , the real MV channel reflection coefficient, Γ_L , and its input impedance, Z_L (Figure 38), can be deduced by deembedding the coupler behavior from the measured Γ_{IN} (Appendix A.3 Appendix A.).

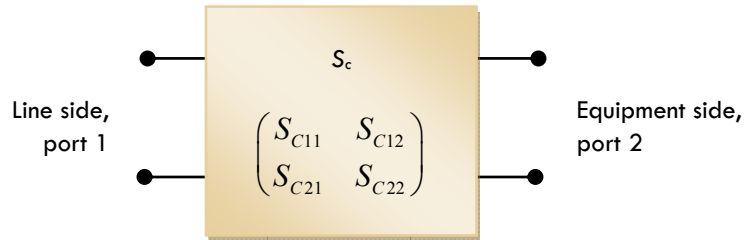


Figure 37 MV coupler S parameters

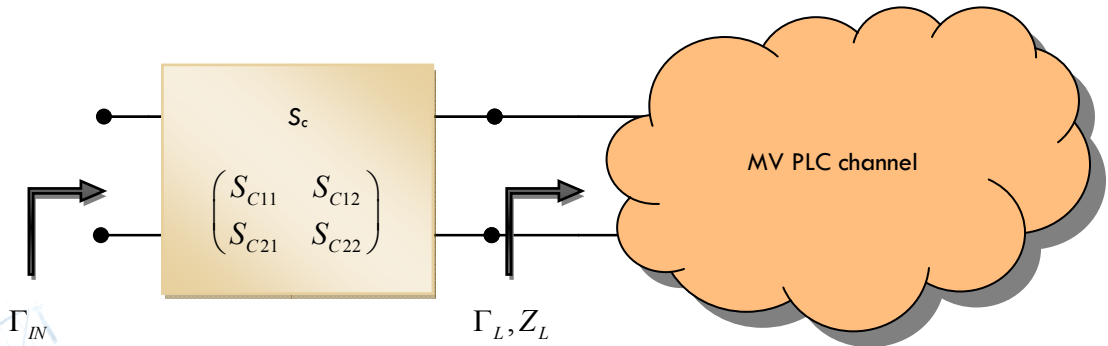


Figure 38 Measured and real reflection coefficient

Figure 39 shows that for our measurement scenario, channel input impedance real part ranges from 12 to 20 Ω , with no variations over time.

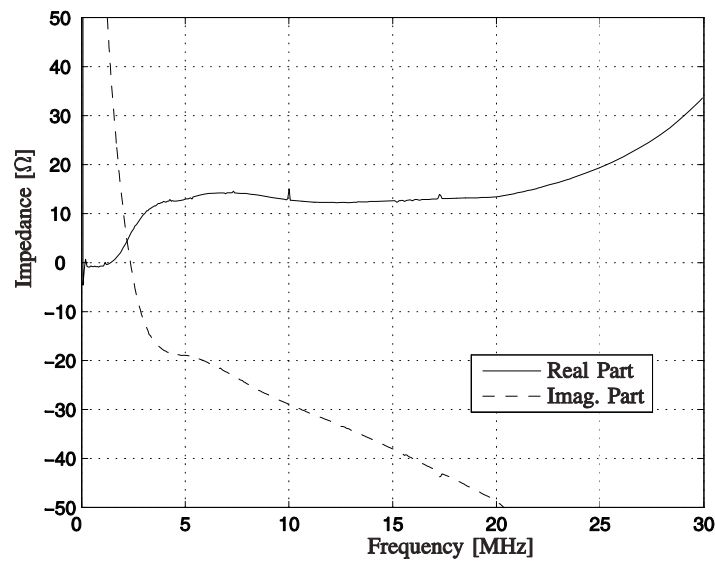


Figure 39 MV channel input impedance

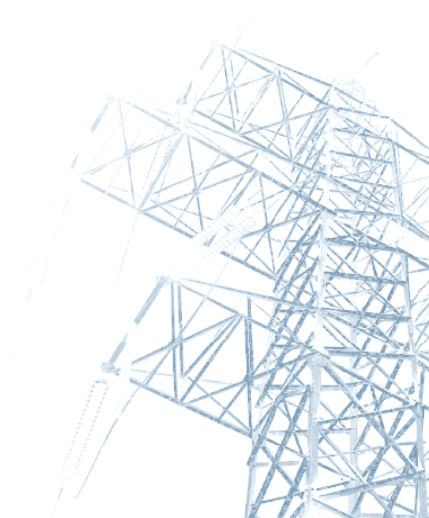
4.4. MV CHANNEL TOPOLOGY MODELING AND VALIDATION

In some channels, like the LV grid, the network topology is complex, very branched, and often, unknown. This kind of environment calls for a stochastic modeling, usually based on multipath models. This is not the case for the MV network, where:

1. The topology is known.
2. The network device characteristics are known.

In this scenario, another kind of modeling can be carried out, i.e., deterministic modeling. This work proposes an ad-hoc modeling for every kind of MV network, or a subset of, based on previous S parameter characterization of network devices.

With this approach, given a network topology and the easily measured device S parameters, the transfer function can be easily obtained from and to any points of the network. This approach is very versatile, since the model can be exported to different regions where different topologies and/or network devices are used. Once the channel transfer function has been found, the noise scenario can be added by easily tuning some noise model, e.g. Ref. [24], by the noise characterization presented in this work (Figure 40).



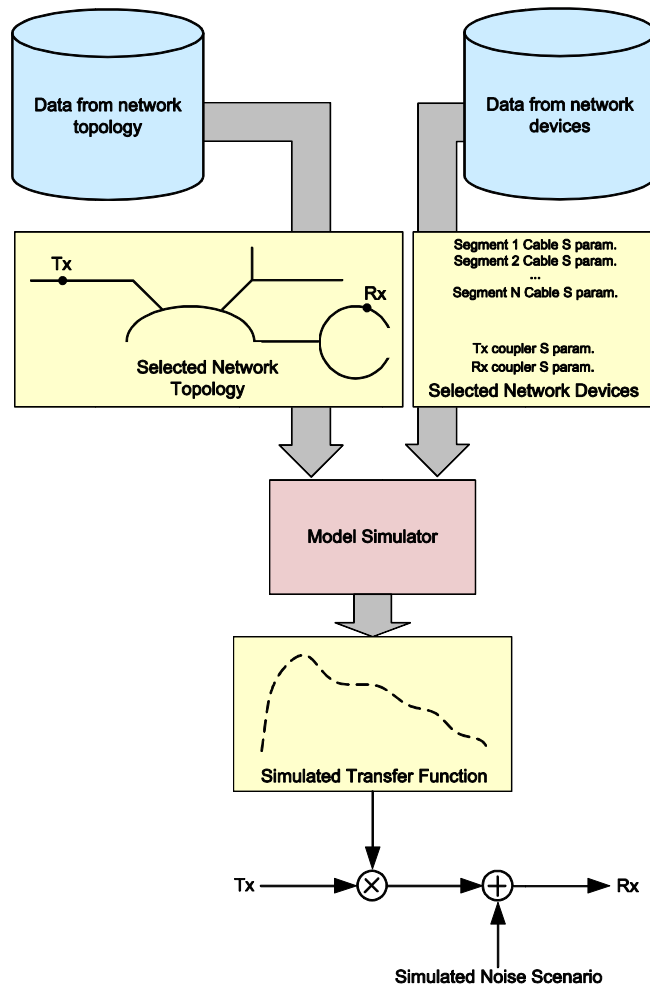


Figure 40 MV model

In order to deterministically model the MV channel topology, the MV distribution cable and coupler have been characterized from structural measurements. The validation of the characterization and the model has been carried out by modeling the real measured network in a circuitual simulator, as shown in Figure 41, and measuring the simulated attenuation characteristic. The modeled network consists of five MV cable segments and four joints between them. These joints are the points where the RMUs are located. In each joint the MV/LV transformer and the coupler can be found, as well as the $50\ \Omega$ impedance of the measurement devices. Although MV/LV transformers are considered perfect barriers for the high frequency signals, they have been circuitual modeled and included in the simulated topology as explained in [81].

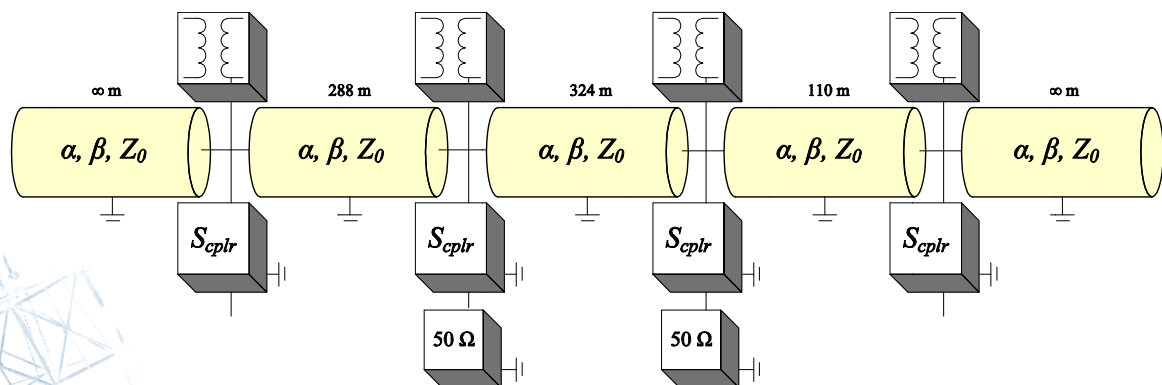


Figure 41 Simulated topology

Figure 42 shows a quite good match between simulation and measure. The deviations between the two characteristics are most probably due to the parasite behavior of RMU elements and physical construction issues, e.g., breakers, structure shapes and sections, and so on.

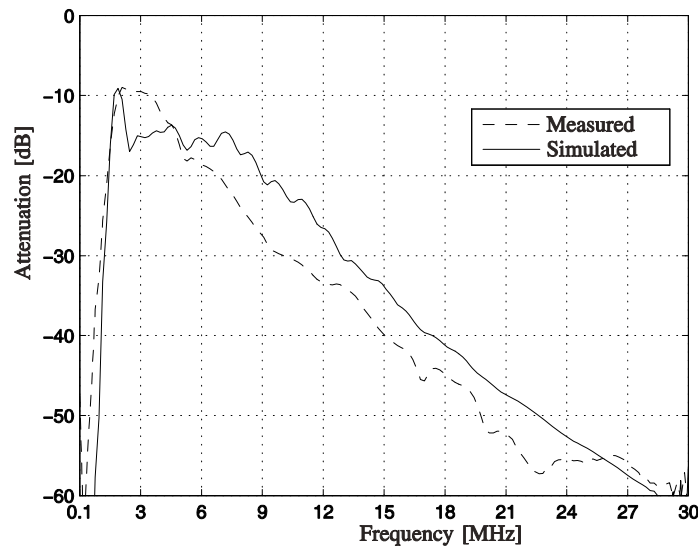


Figure 42 Measured and simulated attenuation characteristics

4.5. CONCLUSIONS

This work has presented seven measurements, two of them for noise characterization and the others to properly model the transfer function of the urban underground MV distribution network. For this kind of scenario, the approximation that best suits this channel is a combination of deterministic and stochastic modeling for the channel transfer function and the noise scenario, respectively.

The scattering parameters based structural characterization of network devices easily yields to the deterministic modeling of an arbitrary network topology, i.e., any kind of topology with any type of components. This is a very powerful approach, since the model can be exported to different regions where different topologies and/or network devices are used while obtaining precise channel transfer functions. Moreover, the structural parameters can be set by statistical values, in order to get the channel behavior for a certain network topology subset or group.

The noise random nature has been characterized, revealing its behavior in time width and interarrival impulse times, as well as the mean and variance for the background noise in the frequency domain. Regarding the noise scenario modeling, the stochastic proposals that can be found in the literature can be easily tuned to meet the MV channel background noise and interference characteristics.

Moreover, a methodology for extracting the value of the network input impedance and its value has been presented, based on the coupler deembedding in order to get an actual channel measure.

CHAPTER 5

5. HIGH VOLTAGE CHANNEL MEASUREMENTS AND MC-SS TESTS

As explained before, Endesa Network Factory S.L. started a physical layer modulation design for HV PLC channels. After measuring the typical MV urban ring channel characteristics (see previous Chapter), the work moved to HV channel measurements and then, based on these measurements, to modulation design.

5.1. INTRODUCTION

Since the beginning of 20th century, the HV network has been exploited as a communications medium. Actually, the first ever running communication equipments on power lines were the HV Double-Sideband Amplitude Modulation (1920s) and SSB-AM modems (1940s). Since no other communications network could offer such a geographic presence, reliability and cost effectiveness; EUs core services, i.e., monitoring, operation management and limitation and removal of failures, were carried out by voice transmission by means of analog PLC systems [4]

In the course of time, voice transmission couldn't achieve the reliability, speed and the level of automation that the EUs deserved for their applications, therefore, a rapid development of PLC systems towards digital implementations shown up.

At the beginning, the digital data transmission was carried out by means of low speed (50 bps) ASK modems. With the increase of the power grid automation level, the needed data rates requirements grew to support the transmission of such a complex system, yielding to the typical 2400 bps modems and the 4 kHz channelization [5][6].

Nowadays, PLC systems are usually based on the combination of the analog and digital modem. This presents a higher degree of flexibility for the EU: while it solves the problem of the DPLC low reliability for tasks such as teleprotection, it overcomes the rate limitation of the analog PLC.

If focusing on data transmission PLC state of the art, the digital systems based on QAM-SCM can reach a net bit rate of up to approximately 80 kbps in a 16 kHz bandwidth with BER below 10^{-6} [7]. MCM begins to play an important role in HV communications. MCM inherent robustness against multipath effects and narrowband interferers, in addition with the high spectral efficiency that can be achieved [16], is making MCM and its most efficient version, OFDM, the choice for manufacturer's next generation HV PLC equipment [8], delivering a data rate of 256 kbps available to the user in a bandwidth up to 32 kHz, extending the usable frequency range up to 1 MHz. Current manufacturer solutions will be discussed in the next section.

Beside the traditional core services mentioned before, EUs would like to satisfy an increasing need of new internal services (support for advanced grid control and automation, audio and video security related communication...), taking benefit from the use of their own power grids [9]. Current standards regarding HV communications are obsolete and unaligned with HV PLC new technology deployment. IEC-TC57 Workgroup 20 recently started to work on the new standard including HV DPLC.

Although the licensed band for PLC is located from 40 kHz to 500 kHz [5][6], in certain situations, the propagation can be favorable enough to use the frequency range above that upper limit; so, the study on this paper will go beyond this constraint and will propose, based on measurements, the exploitation of that range by Cognitive Radio (CR) techniques [68]. While trying to reduce the inference on other PLC equipment in the PLC-licensed band and on the existing broadcast signals on the non-PLC-licensed band, the MC symbol design will have in mind the minimization of the transmitted PSD.

5.2. MANUFACTURER SOLUTIONS

Focusing on data transmission, three main manufacturers rule the HV-PLC world: Siemens, Dimat and ABB [7][8]. Occupying a maximum bandwidth of 8 kHz (in each operating direction) and up to 4 FSK carriers, the Siemens PowerLink can deliver up to $4 \cdot 19.2 \text{ kbps} = 76.8 \text{ kbps}$ of user data rate. The maximum output power that the PowerLink can offer is 60 W of peak envelope power (PEP). On the other hand, based on SC-QAM modulation, Dimat OPD-1 offers 79 kbps available to the user, occupying 16 kHz (in each operating direction), with a maximum output power of 80 W of PEP.

The ABB ETL600 is based on MCM. Occupying a maximum bandwidth (in each operating direction) of 32 kHz and delivering up to 80 W of PEP, the ETL600 is able to offer 320 kbps when the received signal to noise ratio is better than 45 dB. Table 7 summarizes the main HV-PLC modems and their main characteristics.




			
Modulation	FSK	QAM	MC
Maximum user bit rate [kbps]	76,8	79	320
Minimum SNR for max. rate [dB]	35	25	45
Dynamic bandwidth	No	No	No
Quality of service support	Manual, 2 levels, port based	No	No

Table 7 Main HV power line carrier manufacturers

5.3. MEASUREMENT AND TEST SCENARIO

The scenario under test are, in one hand, a 4-circuits, 3-phase 110 kV line between the “Egara” and the “Mas Figueres” Endesa substations, in Barcelona, Spain, both substations separated by 6.85 km (Figure 43); and on the other, a similar 27 km line between the “Sant Celoni” and the “Tordera” Endesa substations, also in Barcelona. In the sequel, the former will be named the “short” and the latter the “long” link. Both channel measurements and data transmission tests have been carried out by the same equipment: two National Instruments PXI chassis. Each chassis consists on an industrial embedded computer, one high stability reference clock [69] and a special instrumentation card. At the transmission, this instrumentation card is a high speed arbitrary waveform generator, capable of output data at 100 Msps at 16 bits of vertical resolution; the receiver chassis has an analogous 14 bits high speed digitizer [70][71]. Both chassis have been synchronized by means of a high resolution (better than 1 μs) pulse per second GPS signal.

